UNIVERSITAT DE BARCELONA

Development and optimization of a Low Temperature Co-fired Ceramic suspension for Mask-Image-Projection-based Stereolithography

Joana Gonçalves Fernandes

FORMULATION OF PHOTOCURABLE LTCC SUSPENSIONS

CHAPTER III

The development and optimization of the LTCC photocurable suspensions of MIP-SLA AM technology is presented in this chapter. Taking into consideration in this optimization was the maximization of the solid load, the optimal dispersant, and the dispersing time. In addition, the effect of both solid load and particle size distribution was studied regarding the rheological behavior and photocuring behavior.

3.1. Introduction

3.1.1. Ceramic suspensions

As explained in previously, the majority of ceramic-forming technologies start with a ceramic suspension. These suspensions are mainly composed of ceramic particles mixed in a liquid medium, a proper dispersant, and further additives that can be added such as binders, plasticizers and anti-foaming agents. The preparation and understanding of the suspension is crucial to succeed the following phases for the whole process: printing, de-binding and sintering processes. Any inhomogeneity in the ceramic suspension, such as density gradients, air bubbles, or presence of agglomerates/aggregates, is a potential defect in the final sintered part.[1]

The aggregates (strongly bound between particles) or agglomerates (weakly bound between particles – van der Waals forces) can be found in most starting powders. Therefore, during preparation, the ceramic suspension must be broken down to avoid heterogeneities, which could result in pore formation or even in differential shrinkages in the sintering step. Their elimination requires a de-agglomeration and dispersion, generally carried out by a milling process applied directly to the starting (dry milling) powder or to the suspensions with its components (wet milling). [2] Figure 3.1 shows the relative stress intensity needed for fragmentation of the agglomerates, aggregates, and primary particle breakage. The breaking of the primary particles linked with solid bonding is called true grinding.[3]

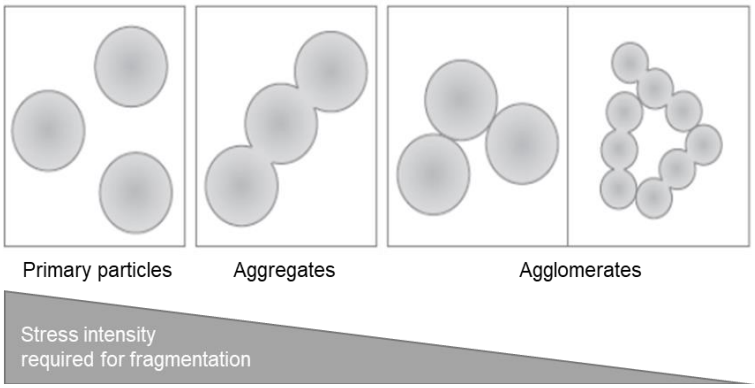

Figure 3.1 – Particle structures and stress intensities required for its fragmentation. Adapted from [3]

In general terms, the dispersion of a powder in a liquid phase involves three main stages: wetting, de-agglomeration, and stabilization. [2]

In the first stage of the dispersion, the wetting of the powder surface by the liquid results in the substitution of solid/gas interfaces by solid/liquid interfaces.[4] As stated previously, the ceramic suspension process needs a de-agglomeration stage, which refers to the breakup of interparticle bonds in the aggregates/agglomerates into elementary particles. Capillary pressure of the solvent in the pores can destroy certain agglomerates with weak bonds, however the ones with stronger bonds may require an activation procedure, which can be obtained by impacts with a milling process, for example. For this to happen, the applied force during the de-agglomeration process has to be larger than the forces between the particles in the agglomerates.[1] The final stage is the stabilization of the ceramic suspensions, which refer to the control of the sedimentation and re-agglomeration of the particles that is determined by the balance of the forces acting between individual particles.[4]

When a powder is dispersed in a liquid, van der Waals forces are developed spontaneously, which are strong and long-range attractive forces. The stabilization of the particles within the dispersion medium requires the development of repulsive forces that allow the particles to be surrounded by the liquid medium and avoid contact between them. This can be achieved by acting in different ways on the forces between the particles, which gives rise to the two general mechanisms of stability: electrostatic repulsion, derived from the interaction between charged surfaces, and polymeric stabilization, provided by the presence of high molecular weight molecules. [5]

In aqueous systems, the surface potential of ceramic particles is strongly dependent on the pH, in this way the ceramic particles can be stabilized by adjusting the pH of the suspensions - electrostatic stabilization.[3] The developed charges at the solid-liquid interface leads to the formation of an electrical double layer surrounding each particle, and consequently the interaction of these electrical double layers gives rise to mutually repulsive forces, keeping the particles separated.[6] In many ceramic systems the stability of the suspension is not possible by electrostatic stabilization, one example being in non-polar organic solvents.[7]

In this sense, the addition of suitable polymeric additives could be used for the stabilization of the suspension. [1] These additives may migrate to the solid-liquid interfaces forming a layer with a sufficient thickness to provide repulsive forces between particles, therefore they can play an important role in the three stages of the ceramic suspension procedure.[2] On one hand, the particles wetted by the liquid phase may not reach much dispersion if no repulsive forces are present between the particles, due to the van der Waals attractive forces. [1], [4] On the other hand, the de-agglomeration stage is more effective by adding these kinds of organic additives and it aids to achieve a stable suspension, avoiding the re-agglomeration and sedimentation of the suspension. [2] The polymeric stabilization can be caused by the presence of free polymer molecules in the medium - stabilization by depletion - or due to the absorption of polymers onto the surface of the particles - steric mechanism. In addition, the polymers can be charged, resulting in a mechanism in which electrostatic repulsion and steric hindrance combine - electrosteric mechanism. These charged polymers are known as polyelectrolytes; one example is ionic surfactants. [8]

The well-known DLVO theory considers the balance of the electrostatic repulsions and van der Waals attractions, explaining the tendency of particles to agglomerate or separate by the combination of both involved forces.[9] This theory has been successfully applied to aqueous suspension stability, nevertheless in no-aqueous systems the low dielectric constants of organic solvents result in weak electrostatic interactions. As a result, electrostatic stabilization is not effective in non-aqueous suspensions, instead, electrostatic stabilization plays the major role in non-aqueous systems.[4], [6], [10]

In this work the dispersing medium of the ceramic suspensions is on acrylic-based photopolymer, to give rise to the construction of the green body during the printing process. In this sense the stabilization mechanism must be by electrostatic forces. Based on the literature, the stabilization of the ceramic suspensions could be achieved by adding a phosphate ester when the dispersing medium is based on acylates resins.[6], [11], [12] The effectiveness of the dispersant can be determined by rheological analysis, once the viscosity of ceramic suspensions is strongly dependent on the particle interactions. In this regard, he minimum viscosity as a function of dispersant amount gives an indication of the higher stability of the system for a certain dispersant. [13]

As mentioned above, during the preparation of the ceramic suspension, energy may be applied to increase the homogeneity of the suspension, by the de-agglomeration of the particles and aiding the adsorption of the dispersant onto the particle surface. One strategy could be by using a milling process, which at first instance contributes to the dispersion and homogenization of the ceramic suspension. However, a particle size reduction could be observed as well. There are different types of mills, such as ball mill, planetary mill, attritor ball mill, rolling mill, and basket mill.[14], [15] Likewise, there are several variables which can influence the milling process, such as type of mill, milling time, temperature of mill, ball materials, mill charge, ball to powder ratio, etc.

In this work two different milling technologies were used: the planetary mill for small batches and the ball mill to scale-up the ceramic formulation. In the case of the planetary mill, the forces acting on the balls is achieved by the combined action of two centrifugal fields, i.e., the charge inside the vials performs two relative motions: a rotary motion around the mill axis and a planetary motion around the vial axis. In this sense, the energy density in these mills is 100–1000 times higher than the energy density used in the ball mill, where the jar is rotating on a horizontal axis. [15]

3.1.2. Rheology

The rheological behavior of ceramic suspensions is used to determine the degree of dispersion, governed by the interparticle forces. A proper dispersion allows to load the suspension with a higher amount of solid particles. In the top-down MIP-SLA machine, the viscosity of the LTCC photocurable suspensions should not have a value higher than 5 Pa·s at low shear rates, [16]–[19] due to the recoating system better explained in the next chapter. The viscosity can be influenced by variables like the nature of the substance, temperature, pressure, shear rate, shear time, and even electric and magnetic fields.

In Newtonian fluids, the flow behavior can be described with a simple linear relation between shear stress, τ in Pa, and shear rate, $\dot{\gamma}$ in s^{-1}. This relationship is known as Newton's law of viscosity, where the proportionality constant η is the viscosity of the fluid in Pa·s (equation 3.1.). [5]

$$\tau = \boldsymbol{\eta} \cdot \dot{\gamma} \qquad (equation\ 3.1.)$$

As a result, a plot of shear stress versus shear rate shows a linear increase in stress with increasing shear rates, where the slope is given by the viscosity of the fluid. In other words, the viscosity of Newtonians fluids will remain constant regardless of the shear rate. Nevertheless, most fluids are non-Newtonian, which means that their viscosity is dependent on shear rate. In this way, the function $\eta(\dot{\gamma})$ can be defined as apparent viscosity. If the viscosity tends to decrease as the shear rate increases, the non-Newtonian behavior is known as shear thinning or pseudoplastic. On the other hand, when viscosity increases with the shear rate, it is called a shear thickening behavior, also known as dilatant. [5]

The Herschel-Bulkley model introduces the yield stress τ_0 in Pa, which is defined as stress that must be applied to the sample before it starts to flow, defined by equation 3.2:

$$\tau = \tau_0 + K \cdot \dot{\gamma}^n \qquad (equation\ 3.2.)$$

where K and n are constants called consistency index and flow index, respectively. This model is valid for a wide range of materials, since the other rheological behaviors can be considered as particular cases of this model[5], as shown in Table 3.1.

Table 3.1 – Particular cases of the Herschel Bulkley model, adapted from [5].

Rheological behavior	**K**	**n**	τ_0
Pseudoplastic with yield stress	> 0	0 < n < ∞	> 0
Newton	> 0	1	0
Pseudoplastic	> 0	0 < n < 1	0
Dilatant	> 0	1 < n < ∞	0
Bingham plastic	> 0	1	> 0

Figure 3.2 shows a scheme of the mentioned cases, for a better visualization of this rheological behavior.

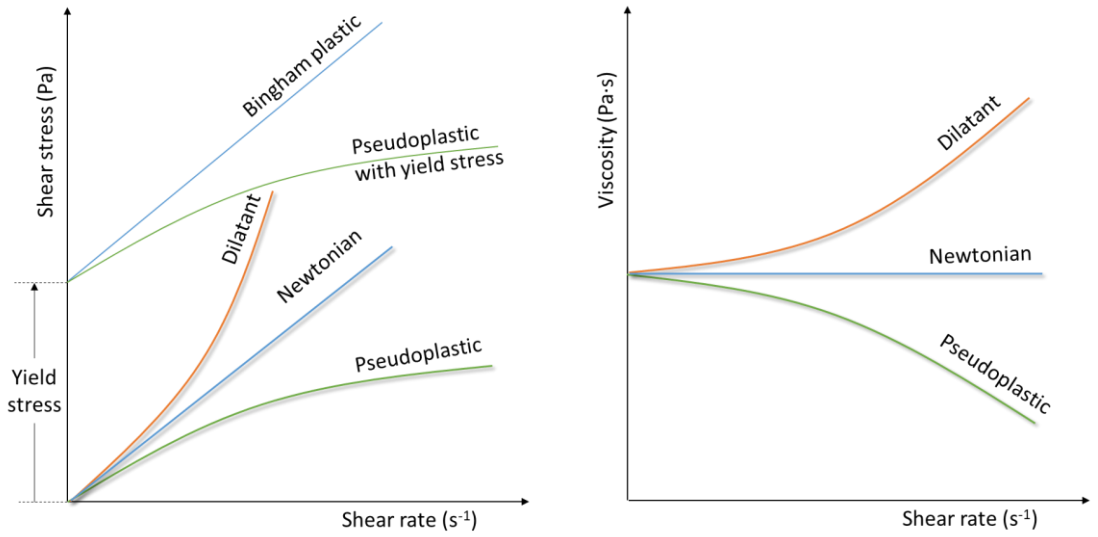

Figure 3.2 – Rheological behaviors.

The rheological behavior of the resin is modified by adding the ceramic load, increasing drastically the viscosity of the new system which will depend on the surface chemistry, particle size, particle size distribution, concentration, and dispersion of the ceramic particles. Besides, to avoid settling of the particles during the printing process, and subsequently to achieve a good homogeneity of the green body, the suspensions must exhibit a pseudoplastic behavior. [17]

However, in a highly loaded ceramic suspension, viscosity increases drastically and makes it inconvenient to handle. This occurs due to the interparticle attraction between the neighboring particles. The repulsive interparticle forces induced by the dispersants create stable ceramic suspensions by reducing the van der Waals forces between particles and, thus, decreases the viscosity. Therefore, the rheology of the suspension plays an important role in studying the ceramic suspension stability. [20]

3.1.3. Photocuring behavior

In a photopolymerization reaction, a resin is hardened when exposed to an energy source such as ultraviolet (UV) or visible light. There are two types of reaction mechanisms: free radical mechanism – usually through double or triple bonds of (Meth)Acrylate - and cationic mechanism - through epoxy groups. As mentioned before, in this case, an acrylic-based resin was used as a dispersing medium.

Curable resins contain a photoinitiator and monomer species, such as vinyl, acrylic, and methacrylic groups. The photopolymerization phenomena are mainly explained by three basic steps: initiation, propagation, and termination. The initiation process occurs when the resin is exposed to light. In this step, the photoinitiators present in the photocurable resin absorb the photons of a certain wavelength generating highly reactive free radicals. During the propagation process, the radicals, previously generated, activate the polymerization by reacting with carbon double and triple bonds of the monomer. This results in a radical monomer which grows by successive reactions with other monomer molecules. Finally, the termination process happens when the end of one radical monomer chain links with another. [21]

Figure 3.3 shows the overall of the photopolymerization in a generic case.

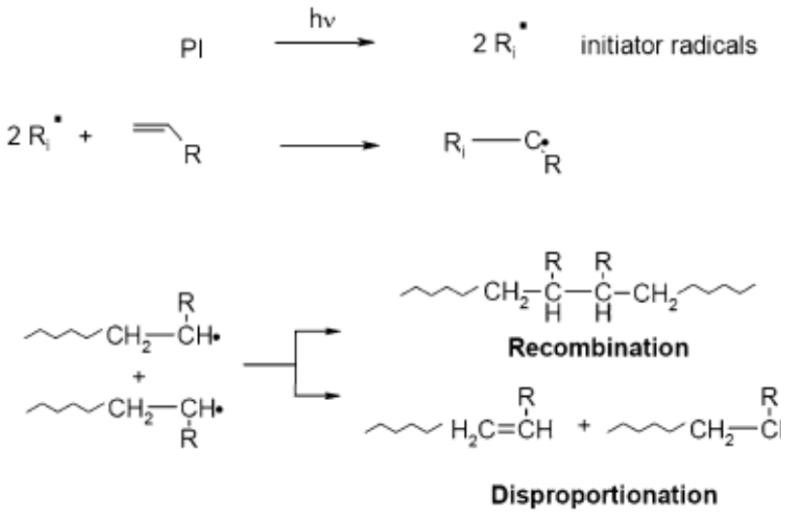

Figure 3.3 – General photopolymerization reaction. Adapted from [21].

For the AM of ceramic pieces based on vat photopolymerization process, the resin must be loaded with the ceramic particles, at least with a 40 vol.%. During the printing process, the photocurable resin is polymerized, trapping the ceramic particles on the crosslinked polymeric matrix, resulting in the green body (ceramic and polymeric matrix). In this work, an acrylate-based resin was used and it is known that the presence of oxygen will inhibit the polymerization process in the free radical mechanism. When a radical reacts with an oxygen molecule, peroxide species (incapable of reacting with monomer molecules) are formed. As a result, the propagation reaction could be stopped by the presence of oxygen molecules. Consequently, the propagation reaction starts only after most of the oxygen species are consumed.[22] Once the MIP-SLA printer used in this work has a top down approach, the upper resin surface is exposed to the air; thus, if a low energy dose is applied, photopolymerization does not occur, or it could cause an incomplete curing.[23]

Apart from the oxygen inhibition, which must be taken into consideration mainly in top-down approaches, there is a minimum applied energy to induce the hardening of the resin. When the applied energy is not enough to overcome the gel point, the hardness of the resin does not occur. The gel point is associated to a certain monomer conversion (α), usually

around 20 %. The energy dose needed to reach the monomer conversation at the gel point (α_{gel}) is defined as critical energy dose, E_c. [24]

A higher energy dose leads to a higher monomer conversion; therefore, the polymer hardens as the degree of polymerization increases. There is a maximum of monomer conversion which is reached at an energy dose maximum (E_{max}), usually around 80% of the monomer conversion. In this regard, although the reaction is not complete, energy doses larger than E_{max} do not cause further reaction, explained by the slow kinetics reaction. [24]

The relationship between the cure depth, C_d, by means of the resultant cured thickness caused by a certain applied energy dose, E_0(mJ/cm^2), is described by the Jacobs equation[25]:

$$C_d = D_p \ln\left(\frac{E_0}{E_c}\right) \qquad (equation\ 3.3)$$

Where the D_p is the sensitivity in the depth direction (the distance at which the laser intensity is reduced by 1/e), which has units of length and is related to an attenuation of the light through the z direction. The relation between C_d and E_0 is commonly presented as a semi-logarithmic plot of C_d versus E_0 dose in logarithmic scale, where:

(1) the semi-logarithmic plot should result in a straight-line relationship, known as the working curve.
(2) the slope of the working curve is exactly the sensitivity, D_p, of the resin.
(3) the intercept of the working curve, i.e., the value of E_0 where $C_d = 0$ is precisely the critical energy dose, E_c(mJ/cm^2), of the resin.

D_p and E_c, are two characteristic constants of the resin with a certain composition and for a certain energy source. When the photopolymerization process is performed by the projection of 2D image, E_0 is calculated based on the energy density (mW/cm^2) and the exposure time (s) for each projected layer.

In the case of loaded resins with ceramic particles, the sensitivity of the resin, D_p, is proportional to the average particle size (d) and inversely proportional to the ceramic volume fraction (Φ) and the materials' scattering efficiency (S).[26] The sensitivity could be described by equation 3.4.

$$D_p \propto \frac{d}{S}\frac{1}{\Phi} \qquad (equation\ 3.4)$$

There is no simple closed-form expression that describes S for concentrated ceramic suspensions. Nevertheless, experimentally S increases with both, ceramic volume fraction and with the refractive index difference between the ceramic and the liquid, for a UV light source.[24]

In this regard, the presence of ceramic particles reduces the polymerization reaction by diluting the photoactive medium and attenuating light by scattering (reflection of the light by the particles). However, reflection of light will not occur when the refractive index of the ceramic load is almost the same as the refractive index of the resin. The higher the refractive index of the ceramic particle, the higher the scattering of light, reducing the curing depth. Thus, materials with low refraction index, such as SiO_2 or Al_2O_3, are more favorable for the photopolymerization process than the ones with higher refractive index such as ZrO_2 or SiC. Besides, by decreasing the particle size, the scattering terms increases, reducing C_d, and once more scattering centers are created, while the volume of the suspension stays constant. [27]

To summarize, the objectives of the formulation of the LTCC suspension are described below:

(1) obtain a pseudoplastic behavior with a viscosity lower than 5 Pa·s at 2 s^{-1} of shear rate, for at least 40 vol.% of solid load. [16]–[19]

(2) In terms of photopolymerization behavior, E_c should be as low as possible to minimize the printing time, and

(3) C_d must be larger than 150 µm to avoid delamination between layers for printing layer of 25 µm thickness [28], for acceptable exposure time (less than 15 s per layer).

Table 3.2 shows different ceramic suspensions based on acrylate resins and its photocuring characteristics.

Table 3.2 – Ceramic suspension formulation and photocuring behavior.

Ceramic filler	Particle size (µm)	Particle concentration (vol%)	D_p (µm)	E_c (mJ·cm^{-2})
Silicon dioxide (SiO_2)	3.5	50-60	140	6.15
Alumina (Al_2O_3)	10	53	75	9.3
Alumina (Al_2O_3)	4.4	50-60	68	4.8
Silicon Nitride (Si_3N_4)	0.5	30	20	C_d = 40 at 2600 mJ·cm-^{2}

3.2. Experimental procedure

In this section, the materials used for the development of the low temperature co-fired ceramic (LTCC) photocurable suspensions are described. Regarding the materials characterization, the photocuring measurements are presented since it is a customized method for the resins characterization which simulates the printing process in the MIP-SLA machine.

3.2.1. Materials

The ceramic suspension has a minimum of three components: resin as the dispersing phase, ceramic LTCC powder as dispersed phase, and a dispersant. The Multitrope 1214 from Croda was used as a wetting agent and dispersant, to increase the homogeneity and reduce the agglomeration of the ceramic particles. This organic additive is a biodegradable anionic surfactant based on the phosphate ester of a natural fatty acid (polyoxyethylene alkyl ether phosphate).

Initially, some commercial resins used for common SLA and/or MIP-SLA systems were analyzed. Their characterizations, in terms of both rheological and photocuring behavior, were considered to properly select the one which will be used as a dispersing phase in the ceramic suspensions. The five studied commercial resins are described in Table 3.3.

Table 3.3 – Commercial resins used for SLA and MIP-SLA machines.

Commercial name	Manufacturer	Characteristics
SPOT IC	Spot-A Materials	Resin suitable for jewelry and dental casting. Yellow coloration
SPOT LV	Spot-A Materials	Extra low viscosity resin. Clear coloring
WAX CAST	Maker Juice Labs	Direct Investment Casting applications such as jewelry, digital dentistry, and engineering models. Red coloration
Standard Blend	Fun To Do	Standard resin used in DLP technology. Yellow coloration
Castable Blend	Fun To Do	Castable resin. Moldable resin designed to melt pieces in bronze, copper, tin or iron. Red coloration

For the resin characterization, the resins are called by their commercial name, except for the two resins from Fun To Do, which will be denominated as Fun To Do for the Standard Blend and Fun To Do Cast for the Castable Blend.

The LTCC used in this work was provided by Heraeus with a powder reference 51528 B, mainly composed of a glass phase and alumina. In Table 3.4 some of its characteristics are presented.

Table 3.4 - LTCC characteristics.

Characteristic	Value
Density ($g \cdot cm^{-3}$)	3.10 – 3.50
Particle size – d_{59} (µm)	2.5 – 4.0
Specific surface area (m^2/g)	> 3.0
Sintering temperature (°C)	870

Figure 3.4 shows the SEM images of the LTCC powder. The presence of the agglomerates with diameter larger than 50 µm can be observed, highlighting the need of a de-agglomeration of these particles during the preparation of the suspension. In addition, the size and morphologies of the particles are very varied and non-homogeneous which could be a drawback in terms of suspension stability, once the sedimentation processes will occur at different rates.

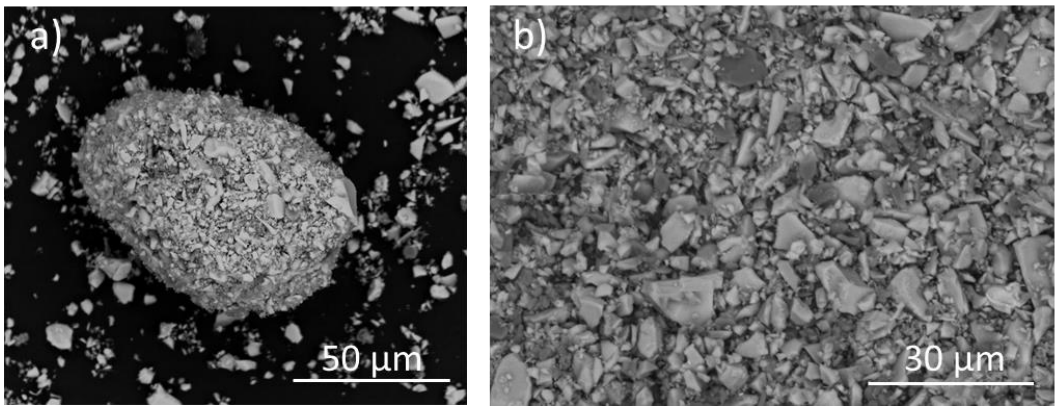

Figure 3.4 – SEM image a) agglomerate b) particle size distribution of the LTCC powder.

3.2.2. Photocuring measurements

The photocuring characterization was carried out in a simplified system, using the same light source as the one used in the MIP-SLA machine. The experimental setup is shown in Figure 3.5, which identifies elements such as the visible light projector, a computer to give the instructions for the projection, a transparent substrate and a vat containing the resin or LTCC suspension. The substrate is not used in the printing process, nevertheless it was used to aid the measurement of the cured depth.

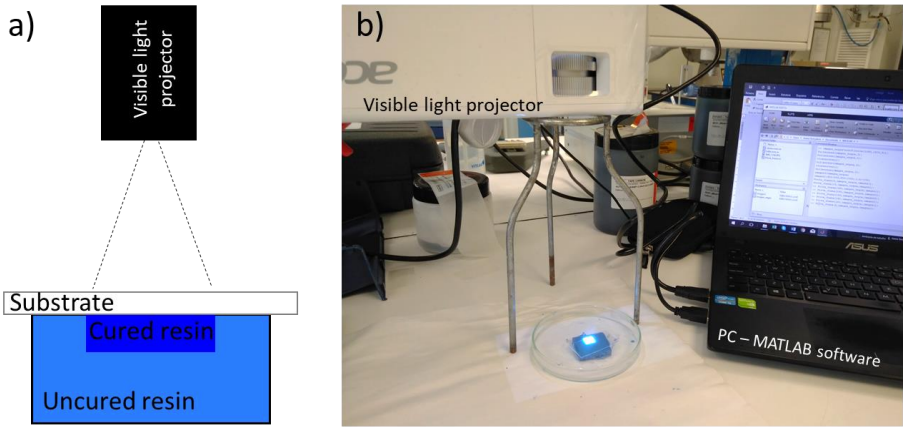

Figure 3.5 – a) a scheme of the experimental setup and b) a real image of the setup for the photocurable behavior

The visible light projector used in the MIP-SLA machines is an Acer H6510BD, based on DLP technology, which has a maximum resolution of 1920 x 1200 pixels and a brightness of 3000 lm using a light source with 210 W (OSRAM lamp).

Given the characteristics of the projector, it is possible to know the energy with which the sample is irradiated. The luminous efficiency of this projector is 14.2857 $lm \cdot W^{-1}$, which is calculated with the brightness value divided by the power of the lamp. This corresponds to a luminous efficiency of 2.0919%, estimated value at a wavelength of 555 nm where 1 lm corresponds to a 683 W. Consequently, the effective power is around 4.3924 W.

However, the light projector is placed at 20 cm from the sample, projecting an area of 167 mm X 167 (9/16) mm. In this regard, the projected energy is distributed throughout the projection area, thus it is convenient to know the irradiance which is 27.9805 $mW \cdot cm^{-2}$. This value means that at each second the projector radiates an energy dose of 27.9805 mJ/cm^2.

The photocuring characterization was analyzed by the working curve of each photocuring system (commercial resins and loaded ceramic suspensions). In this sense, different energy doses must be applied by varying the exposure time to measure the resultant cured depth. This information is fundamental to graph the semi-logarithmic plot of $C_d$vs. $E_0$for each sample. To standardize all measurements, a 2D image of 8.50 mm was projected using the MATLAB program, where the exposure time could be tuned.

Particle size of the raw powder and the suspension was measured using the MASTERSIZER 3000 from Malvern Panalytical, based on laser diffraction technology. In addition, the rheological measurements were carried out on a TA Instruments Discovery HR-1 rheometer with a plate-plate geometry with 40 mm diameter, at 23 ^0C.

3.3. Resin characterization

The five resins were firstly studied regarding both rheological and photocuring behavior. The resin, which will be used as a dispersing medium on the ceramic suspension, will be selected based on the following requirements:

1) The lowest viscosity, once the viscosity of the suspensions drastically increases by adding the ceramic particles.

2) The highest cured depth, once the addition of the ceramic particles leads to an increase of the light scattering, reducing the cure depth.

3.3.1. Rheological properties

In this section the rheological behavior of the five resins is presented. For this study, the viscosity was measured varying the shear rates (flow curves) at room temperature. Figure 3.6 shows the flow curves for the five resins.

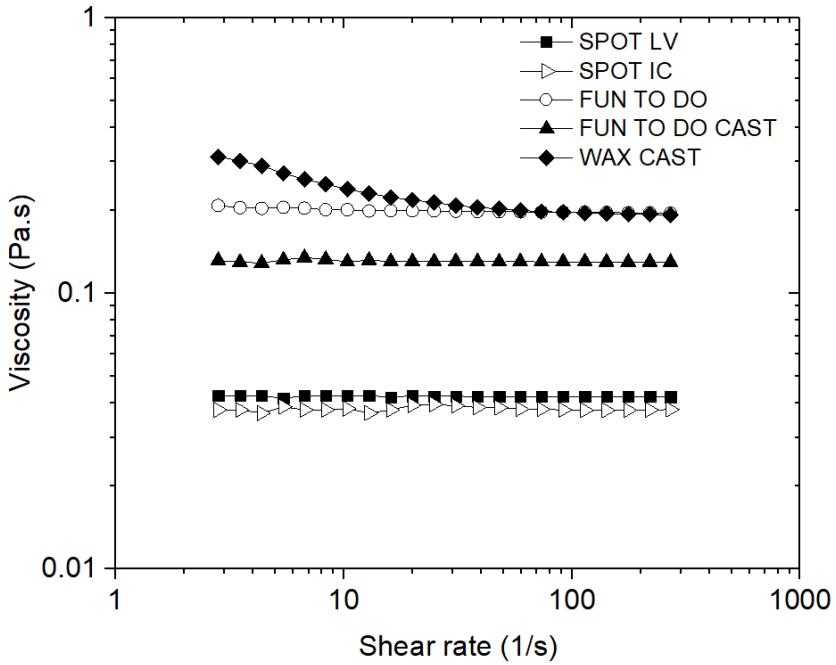

Figure 3.6 – Viscosity vs. shear rate of the different resins.

The viscosity analysis shows that all resins present a Newtonian behavior except the WAX CAST resin, which presents a pseudoplastic behavior. Although a pseudoplastic behavior is a requirement for the ceramic suspensions, the resin does not necessarily have to has this behavior. The rheological properties of the ceramic suspension will be modified with the addition of the ceramic suspensions, thus for the selection of the resin, the main requirement is its low viscosity.

Regarding the viscosity results, the SPOT LV and SPOT IC are the ones with the lowest viscosities, around 40 mPa·s.

3.3.2. Photocuring behavior

In this section, the main objective is the study of the photocuring behavior using the visible light projector as an energy source. This experiment was performed applying different energy doses, i.e., varying the exposure time and measuring the resultant cured thickness (C_d). Therefore, based on equation 3.3, the working curves and, consequently, the characteristic parameters for each resin could be obtained. Figure 3.7 shows the working curves for the five unfilled resins.

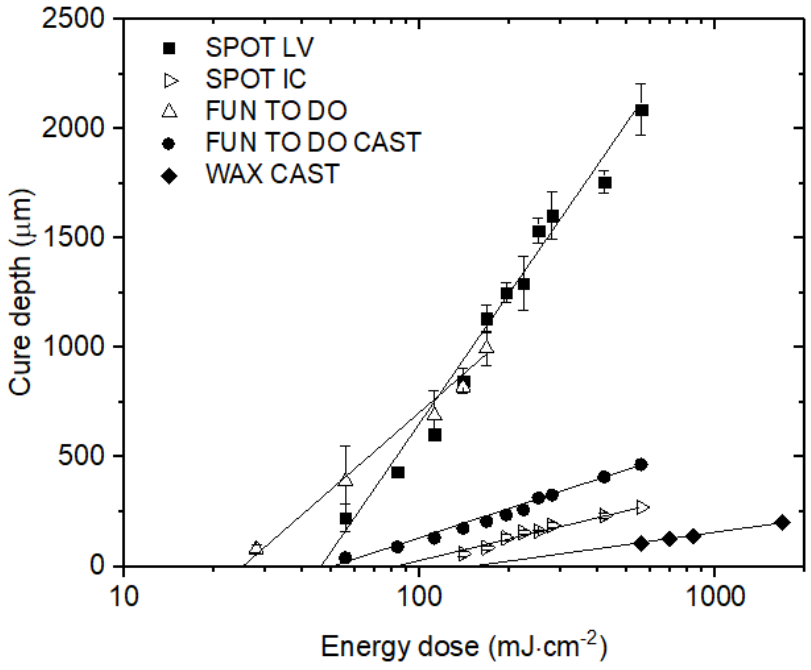

Figure 3.7 – Working curves of different resins.

The slope of the working curve represents the sensitivity, D_p, and E_c is the intercept on the energy dose axis, i.e., the energy required to initiate the polymerization. The obtained values are presented in Table 3.5.

Table 3.5 – Sensitivity and critical energy dose parameters of the resins.

Resin	D_p (μm)	E_c (mJ·cm^{-2})
SPOT IC	151	88
WAX CAST	85	159
SPOT LV	850	48
FUN TO DO CAST	193	53
FUN TO DO	607	27

As shown in Table 3.5, the Fun To Do Cast, SPOT IC, and WAXCAST resins have a very low sensitivity parameter. In the case of the WAX CAST resin, for values lower than 560 mJ·cm^{-2} (20 s of exposure time) the cured layer does not have enough consistency to be measured. In the case of the SPOT IC resin, the same occurs for energy doses lower than 140 mJ·cm^{-2} (5 s of exposure time). Note that the critical energy dose is 88, 159 and 53 mJ·cm^{-2}, for the SPOT IC, WAX CAST, and for the Fun To Do Cast resins, respectively. This means that the gel point (∼20 % of photoconversion) occurs at these energy doses, nevertheless the cured depth is not enough to form a film. On the other hand, the SPOT LV and Fun To Do have sensitivity values of 850 and 607 μm, respectively. These values are much higher in comparison with the other resins, moreover with the lowest critical energy dose values.

As mentioned previously, the requirements for the selection of the resin are (1) the lowest possible viscosity and (2) the highest sensitivity in the visible light range. Thus, the resin which has the lowest viscosity, 42 mPa.s, and the highest sensitivity, 850 mJ·cm^{-2}, is the SPOT LV resin. This resin is an acrylate-based resin with a phosphine oxide-type photoinitiator, with a density of 1.1 g·cm^{-3}.

3.4. LTCC photocuring suspension

3.4.1. Solid load

Once the resin is already selected, the subsequent study is concerning the LTCC load. Therefore, this experimental session is focused on the effect of the solid load on both rheological properties and photocuring behavior of the LTCC suspension.

Regarding the de-binding and sintering processes, the LTCC suspension must contain a high ceramic concentration (> 40 vol.%) to prevent defect formation (cracks and delamination) and to maximize the density of the sintered part. On the other hand, the recoating system of the developed machine is by dipping the part into the uncured resin. This means that the viscosity should be the lowest possible and not higher than 3-5 Pa·s at low shear rates (3 s^{-1}), for a proper recoating.

In this sense, the main objective of the following study is to maximize the ceramic load, taking into consideration the requirements imposed by the printing machine in terms of viscosity and photopolymerization behavior. Consideration for the following analysis:

(1) The terminology of “dispersing time” will be used for the time applied for the dispersion of ceramic suspension in the milling systems.
(2) The percentage of the dispersant is always with respect to the solid load, in weight percent (wt.%).
(3) The solid load could be presented in wt.% or in volume percent (vol.%), always with respect to total of resin and LTCC powder.
(4) The ceramic suspensions was prepared in planetary ball milling in small batches of 50 g, with 5 balls with a diameter of 10 mm .

The LTCC suspensions with different solid loads were prepared using the same dispersing conditions, i.e., 30 min of dispersing time and 1 wt.% of dispersant. Table 3.6 shows the relationship of the solid load in wt.% and vol.%, of all studied LTCC suspensions.

Table 3.6 – Relationship of wt.% to vol.% of LTCC suspension.

Powder load (wt.%)	Powder load (vol.%)
10	3.6
50	25.0
60	33.3
67	40.4
72	46.2
75	50.0

Figure 3.8 shows the viscosity values measured at low shear rate, 2 s^{-1}, for the suspensions with different solid loads.

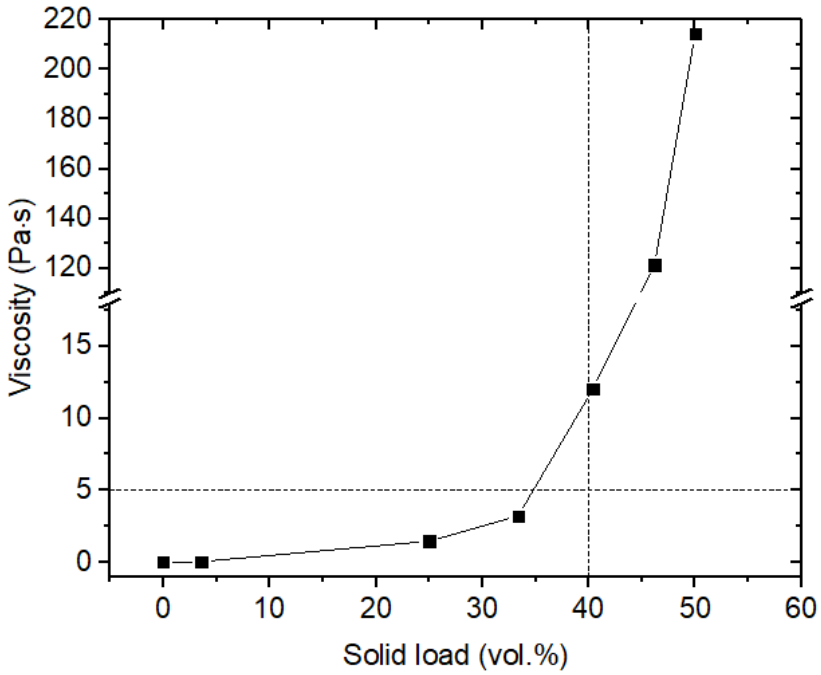

Figure 3.8 - Viscosity measured at a shear rate of 2 s-1 for different solid loads with 1 wt.% of dispersant.

As said previously, there are two main conditions for formulation of the LTCC suspension in terms of viscosity and solid load. These requirements are represented in Figure 3.8 with dotted lines. The horizontal one represents the limit in terms of viscosity, meaning that the viscosity values must be lower than 5 Pa·s and, the vertical one shows the minimum solid load, i.e., 40 vol.%.

The addition of ceramic powder drastically increases the viscosity, being more evident for volume fractions larger than 46 vol.%. For example, the viscosity of the suspension with 40.4 vol.% of LTCC presents a viscosity of 12 Pa·s and by adding less than 6 % of ceramic particles, the viscosity reaches values ten times higher (120 Pa·s).

It is observed that the suspensions with viscosity lower than 5 Pa·s are the ones with a solid load lower than 33 vol.%. Therefore, the two requirements are not achieved with this experiment. However, it is known that the optimization of both percentage of dispersant and dispersant time are two important parameters for the stabilization of the suspension and, consequently, decreases its viscosity. In this regard, a higher solid load can be selected for the further optimization considering these two parameters: amount of dispersant and dispersing time.

The influence of the solid load on the photopolymerization process is also an important parameter for the printing process. In this sense, the following results are related to the polymerization behavior of the suspensions with different solid loads. The following results will give the information about how the ceramic suspensions react with the visible light during the printing process. From now on, the percentage of solid load will be represented in terms of weight.

The working curves for different LTCC load suspensions are presented in Figure 3.9, where the slopes of these curves are the D_p values, and the E_c values are the interception of the energy dose axis, represented in Table 3.7.

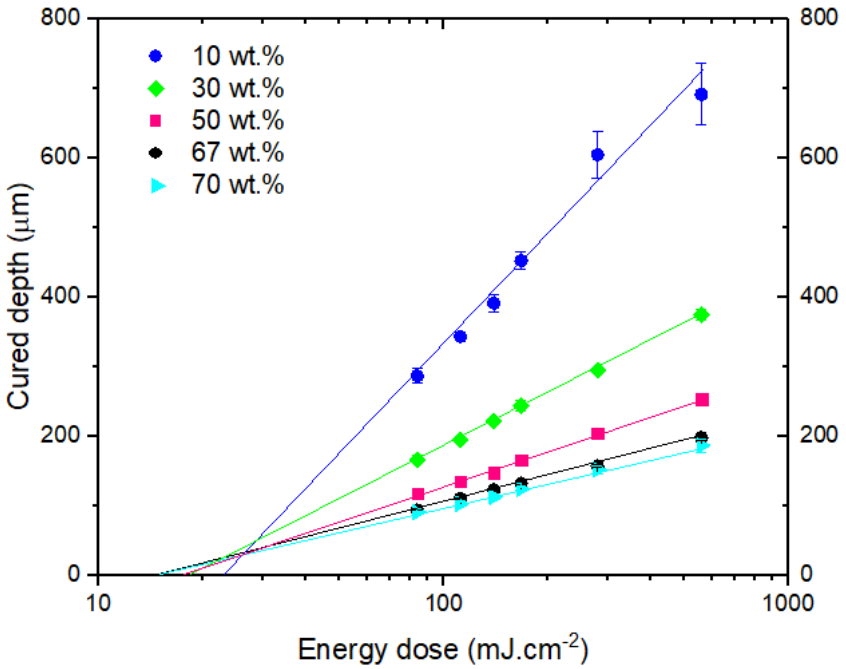

Figure 3.9 – Working curves for different LTCC solid loads (1 wt.% of dispersantt).

Table 3.7 - Critical energy (E_c) and sensitivity o (D_p) values for LTCC suspensions with different powder loadings(1 wt.% of dispersant).

Powder load (wt.%)	Powder load (vol.%)	D_p (µm)	E_c (mJ·cm^{-2})
0	0	850	48
10	3.6	226	23
30	12.5	110	19
50	25	73	18
67	40.4	54	15
70	43.8	52	15

The general analysis of the working curve results shows a decreasing of the slope for the suspension with a higher amount of ceramic particles. This means that the attenuation of the light increases as the solid load increases. Correlating these results to the printing process, if a layer thickness of 150 µm is needed to build up a certain part, the required energy dose will be different depending on the solid load. For example, to obtain a cured layer of 150 µm, the energy dose needed to apply during the printing is 45, 70, 140, 230, and 290 $mJ \cdot cm^{-2}$, for 10, 30, 50, 67, and 70 wt.% LTCC, respectively. This affects directly the printing velocity which will affect the fabrication velocity, however this parameter is not the focus of the suspension optimization.

Regarding the critical parameters of the suspensions, E_c and D_p, even for low powder concentrations (10 wt.%; Ec = 23 $mJ \cdot cm^{-2}$), the value of E_c is reduced to half comparing with the resin itself (i.e. 48 $mJ \cdot cm^{-2}$). In terms of sensitivity, the D_p decreases by 73 %, from 850 µm to 226 µm. This is indicative of the strong influence of the solid load on the photopolymerization process.

Figure 3.10 shows the behavior of D_p and E_c in function of the solid load with the values presented also in Table 3.7.

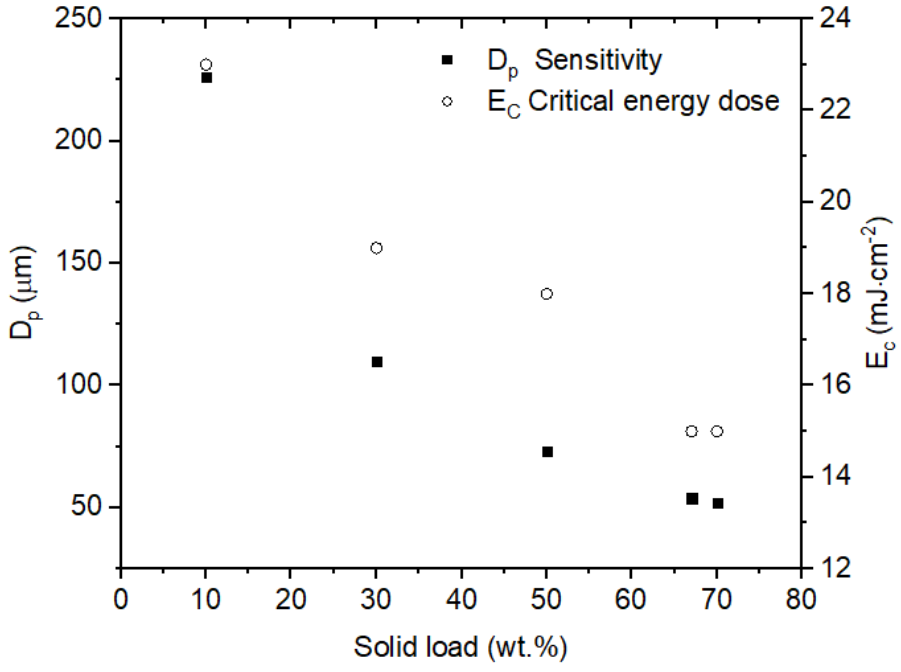

Figure 3.10 – D_p and E_c in function of the solid load of LTCC.

It is observed that the E_c necessary to initiate the photopolymerization process decreases for larger concentrations of ceramic powder, which corresponds to a larger surface occupied by inert particles. This behavior was already reported on alumina suspensions.[12] By substituting the curable resin by inert ceramic particles, the energy necessary for the polymerization decreases. This is also related with the oxygen inhibition that occurs in acrylic systems when printed in a top-down SLA/MIP-SLA configuration. If a lower surface of resin is exposed to the air by increasing the ceramic powder load, a lower energy dose is needed to initiate the photopolymerization reaction.[16] The photocuring behavior tests were performed using a transparent substrate, thus the oxygen inhibition was not considered in these results. However, some tests were made without the substrate, simulating the printing process, and no differences were observed once this effect occurs at a sub-micrometer scale within the measurement error.

Regarding the sensitive parameter, the addition of ceramic particles leads to a decrease of this parameter. This is explained by the scattering of the light by the ceramic particles, which attenuate the penetration of the light, preventing the polymerization process in the depth direction. This means that for the same energy dose, the cured depth of a highly loaded suspension is lower when compared with one with lower solid load. [26]

All LTCC suspensions show appropriate parameters and are also feasible in terms of printing velocity. For example, the samples with 67 wt.% of LTCC needs a 230 $mJ \cdot cm^{-2}$ to cure 150 µm, which corresponds to 4.4 seconds of exposure time for each layer during the printing process.

As already mentioned, none of these samples possess the ideal properties (viscosity lower than 5 Pa·s and at least 40 vol.% of solid load), however it was decided to work with a sample with 67 wt.% (40.4 vol.%) of LTCC with 12 Pa·s at 2 s^{-1}. This viscosity characteristic can and will be further optimized regarding both percentage of dispersant and dispersing time.

3.4.2. Dispersant optimization

As stated before, the homogeneity of the ceramic suspension could be improved by adding the optimal amount of dispersant. The following results are related to the dispersant optimization for the suspensions with 67 wt.% of LTCC, which means 33 wt.% of SPOT LV. The goal is to improve the homogeneity and consequently decrease the viscosity of the LTCC suspension.

The dispersant concentration was optimized for the lowest viscosity of the suspension, ensuring an optimal particle dispersion. Figure 3.11 shows how the dispersant concentration affects the viscosity of the 67 wt.% suspension. These viscosity values were measured at 2 s^{-1} of shear rate, as the LTCC suspension must have a viscosity lower than 5 Pa·s at low shear rates. This optimization was performed by varying the dispersant concentration from 0.25 to 2 wt.% with respect to the powder load, with 30 minutes of dispersing time.

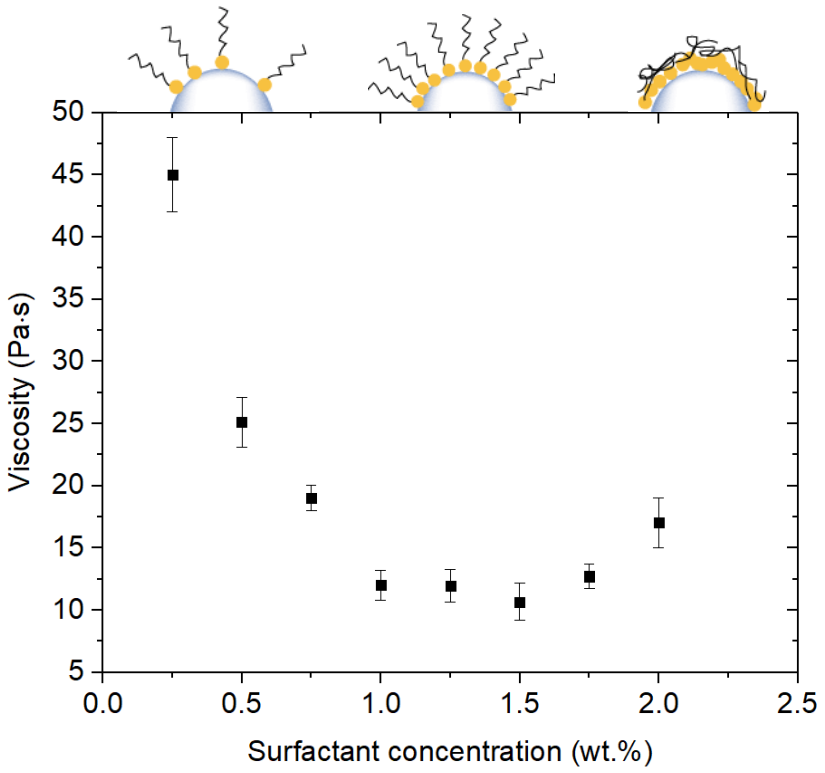

Figure 3.11 – Effect of the surfactant concentration on the viscosity (2 s^{-1}) for the 67 wt.% LTCC suspension.

For low dispersant concentrations, the particles are coated only partially with dispersant molecules, thus the stability and homogeneity of the system is not optimal. As the concentration of the dispersant increases, its molecules completely cover the particles, whereby the viscosity decreases, reaching a minimum which represents the highest stability level; as concentration increases, an increase of interactions between adsorbed chains of dispersant onto the particle surfaces increases the viscosity and the system is no longer in equilibrium.

Figure 3.12 shows the flow curves for three different concentrations of dispersant representing the different behaviors, i.e., before the minimum viscosity (0.75 wt.%), the minimum viscosity (1.50 wt.%) and after the minimum viscosity (2.00 wt.%). The data was analyzed by fitting the Herschel-Bulkley model, equation 3.2, presented in Table 3.8.

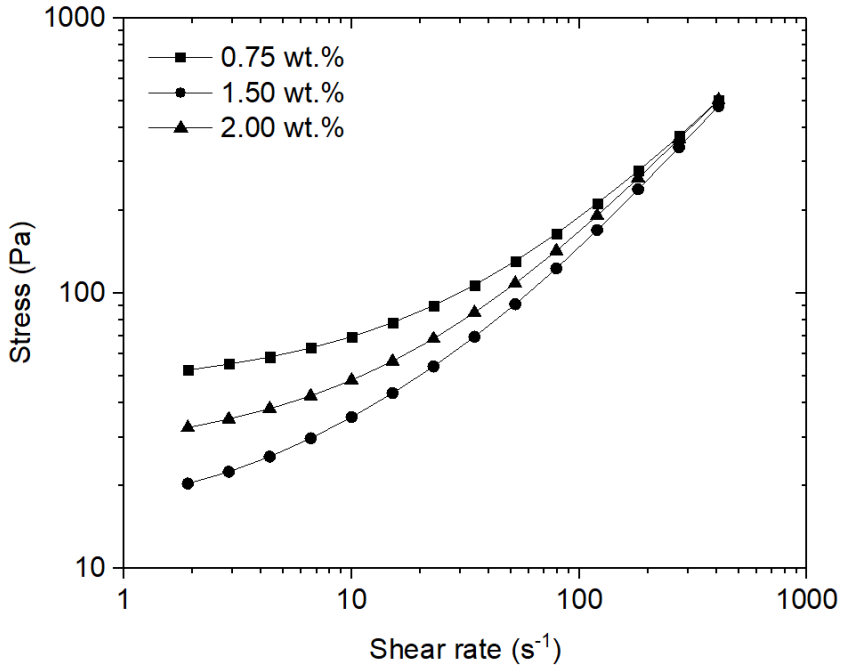

Figure 3.12 – Flow curves for different surfactant concentration, for the 67 wt.% of LTCC.

Table 3.8 - Herschel-Bulkley fitting results for 0.75, 1.50 and 2.00 wt.% of dispersant.

Rheological parameters	Dispersant amount (wt. %)		
	0.75	1.50	2.00
τ_0 (Pa)	48.4 ± 0.4	18.4 ± 0.6	29.1± 0.3
K (Pa·s^n)	3.1 ± 0.1	2.3 ± 0.1	2.5 ± 0.1
n	0.831 ± 0.003	0.899 ± 0.005	0.871 ± 0.003
Adj. R-Square	0.99997	0.99993	0.99998

In all cases the flow index (n) is lower than 1, i.e., pseudoplastic behavior, thus the viscosity decreases when the shear rate increases. This behavior is one of the requirements to prevent the sedimentation of the suspension. Nevertheless, for the 1.50 wt.% the n value is closer to 1, which is related with the least viscosity variation during the flow test (least pseudoplastic behavior).

It Is also observed that for higher shear rates, the viscosity tends to be the same for all formulations, reaching a viscosity limit or plateau. This can be explained because for high shear rates there is a high deformation of the suspension structures involving breaking of aggregates, thus the particles will follow the shear direction.

Analyzing the consistency index (k) and the yield stress (τ_0), the lowest values correspond to the 1.50 wt% of dispersant. As said in the introduction, the yield stress is defined as the force required for a fluid to start flowing, which reflects the resistance of the fluid structure to be deformed. In this sense, it is better to have a suspension with low yield stress for the recoating system. [26]

Thus, it has been concluded that the optimum percentage of dispersant for this system corresponds to the minimum value of viscosity, that means at 1.5 %wt with respect to the solid contents, with a yield stress of 18.4 ± 0.6 Pa and an index flow 0.899 ± 0.005. The optimization of the dispersants leads to a decrease of the viscosity, from 12 to 10 Pa·s, which still does not meet the target of having a viscosity lower than 5 Pa·s. It is expected to achieve target viscosity by optimizing the dispersing time, which is discussed in the following section.

3.4.3. Dispersing time

In order to achieve the required viscosity, the dispersing time was studied in this section. The main objective is to reduce the agglomerates and provide a better absorption of the dispersant onto the particle surface. Until now the dispersing of the suspensions was performed during 30 minutes in a planetary mill, always with the same amount of suspensions and the same proportion of ball to suspension ratio.

In this section the optimized suspension, 67 wt.% LTCC with 1.5 wt% of dispersant, was studied by varying the dispersing time, from 30 to 90 minutes in the planetary milling system. Figure 3.13 shows the viscosity measured at 2 and 100 s^{-1} of shear rate, for different dispersing time. The viscosity values at 100 s^{-1} show that for higher shear rates, the viscosity tends to be almost the same value, meaning that the major differences are observed at low shear rates.

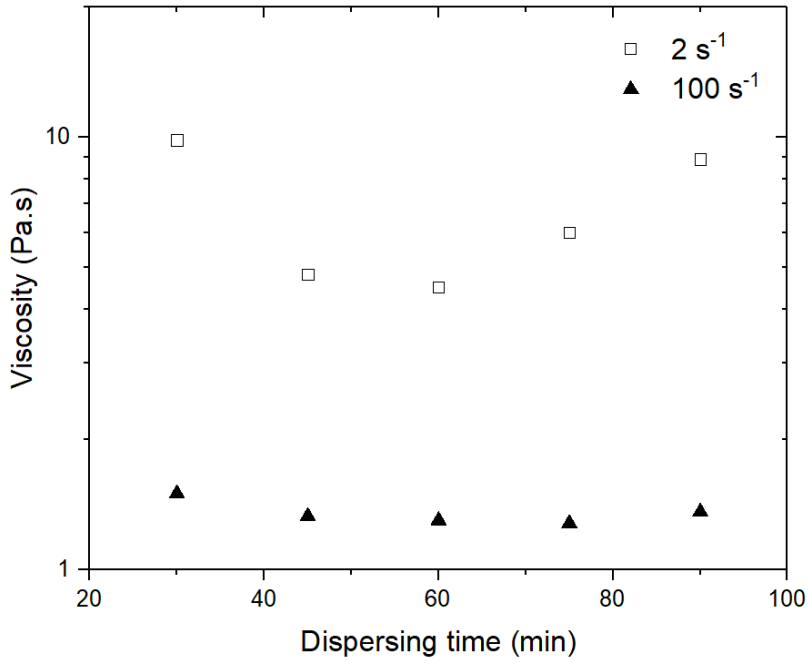

Figure 3.13 – Viscosity versus dispersing time for the 67 wt.% of LTCC with 1.5 wt% of surfactant.

In this study the viscosity plateau is observed; note that the viscosity values of the measurements performed at 100 s^{-1} are almost the same, around 1.3 Pa·s. Analyzing the results at 2 s^{-1}, there is a decrease of the viscosity until 60 minutes of dispersing time and for higher dispersing time the viscosity increases. Thus, between 45 and 60 minutes of dispersing time is the optimal period for the homogenization of the suspensions, with a viscosity between 4.5 and 4.8 Pa·s, respectively. This period corresponds to the maximum absorption of the dispersant onto the particle surface, for a certain particle size/agglomerate size distribution, which reduces the viscosity of the system. The increase of the viscosity for higher dispersing time could be explained with the formation of more superficial area (reduction of the particle size), which decreases the proportion of dispersant to new particle surfaces (a lack of dispersant for the new particles/agglomerates distribution).

Figure 3.14 shows the flow curves for the 30 and 60 minutes of dispersing time; both present a pseudoplastic behavior. It is observed that the viscosity for high shear rates is almost the same, as presented in Figure 3.13. However, for lower shear rates there is a significant change, from 10 to 4.5 Pa·s for the 30 minutes and 60 minutes of dispersing time, respectively. This means a better homogenization of the suspension with 60 minutes of dispersion time.

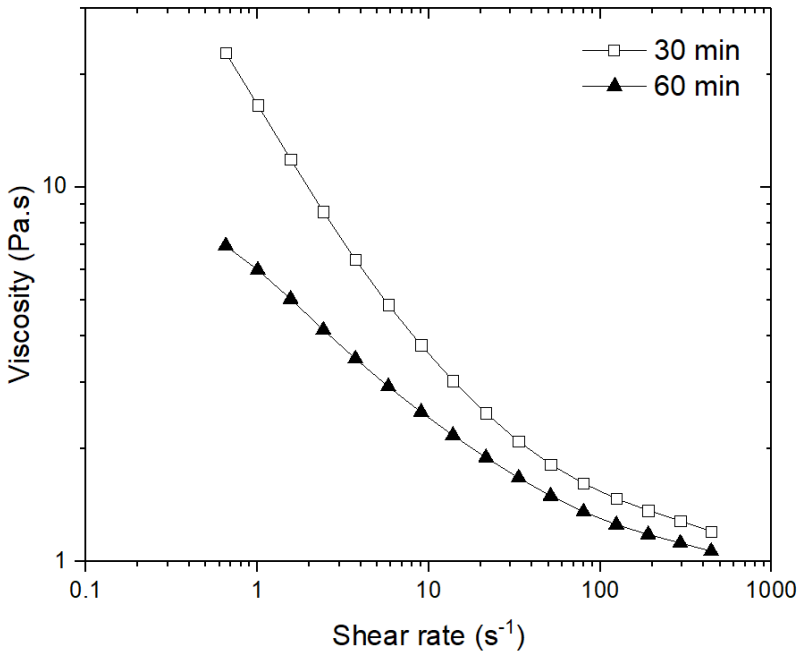

Figure 3.14 – Flow curve for 30 and 60 minutes of dispersing time for 67 wt.% of solid load with 1.5 wt% of surfactant.

Table 3.9 shows the results of the Herschel-Bulkley fitting (equation 3.2) for both samples.

Table 3.9 - Herschel-Bulkley fitting results for 30 and 60 minutes of dispersing time.

Dispersing time (min)	30	60
τ_0 (Pa)	18.4 ± 0.6	5.9 ± 0.8
K (Pa·s^n)	2.3 ± 0.1	2.2 ± 0.1
n	0.899 ± 0.005	0.880 ± 0.007
Adj. R-Square	0.99993	0.99998

By optimizing the dispersing time, the viscosity target was achieved. Moreover, the yield stress decreases from 18.4 ± 0.6 (30 min) to 5.9 ± 0.8 (60 min), which is also favorable for the recoating process.

In this sense, the viscosity and solid load requirements were achieved by optimizing the dispersant concentration and the dispersing time. As a result, a 67 wt.% (40.4 vol.%) of LTCC with a final viscosity of 4.5 Pa·s (at 2 s^{-1}) was obtained by adding a 1.5 wt.% of dispersant and dispersing during 60 minutes in a planetary ball mill.

As stated before, the maximum weight in each crucible of the planetary mill is 50 g, with a maximum of 100 g per batch. However, in the MIP-SLA machine the vat must be completed filled of LTCC suspension once it has a top-down configuration. Consequently, for the printing process, at least 1 L (around 2 kg) of ceramic suspension must be prepared.

Therefore, large-scale production of the LTCC suspension should be considered. In this sense, the milling process must have the capacity to assume a higher volume of suspension.

One possibility to scale up the process is by using a horizontal ball mill, where the volume limit is given by the jar used and the distance between the axes; nevertheless, it always has a higher capacity than the planetary mill. Thus, the following study has the goal of scaling up the fabrication of the LTCC photocurable ceramic suspension using the horizontal ball mill.

3.5. Large scale production

The LTCC suspension which was previously optimized for small batches was used as the main formulation for the scale-up development, i.e., a 67 wt.% of LTCC powder dispersed in the SPOT LV resin, with a 1.5 wt.% of dispersant. The main objective is the optimization of the homogeneity of the suspension regarding both rheological and photocuring behavior in the large-scale production system.

The dispersion study was carried out in a ball mill system during 305 hours (~13 days), to analyze the viscosity and photocuring behavior evolution during the dispersant time. These results are also investigated in terms of the particle size distribution, i.e., how the particle size affects the viscosity and the photocuring behavior.

The preparation of the LTCC suspension was carried out in a polymeric jar, adding all the compounds directly: alumina balls with a diameter of 3 mm, dispersant, resin, and LTCC powder (in this order). It was observed that for times shorter than 5 hours, the suspension was not homogenous, thus, no measurements were performed before 5 hours of dispersing time.

Figure 3.15 shows the jar with all compounds before the dispersion process and the result of the suspension at 5 hours of dispserting time.

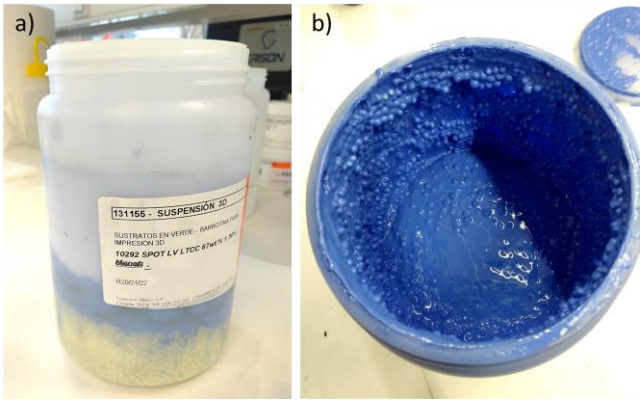

Figure 3.15 – Images of the a) jar with all compounds before the dispersion process and b) LTCC suspension at a dispersing time of 5 hours.

3.5.1. Influence of t dispersing time on viscosity

In this session, the viscosity of the LTCC suspension was measured at different times during the 305 hours. The samples were removed from the jar at different times for the measurement of the viscosity and particle size distribution.

The flow curve was measured for each sample. Figure 3.16 shows the viscosity values at 2 s^{-1} of shear rate, which is the reference in terms of viscosity value.

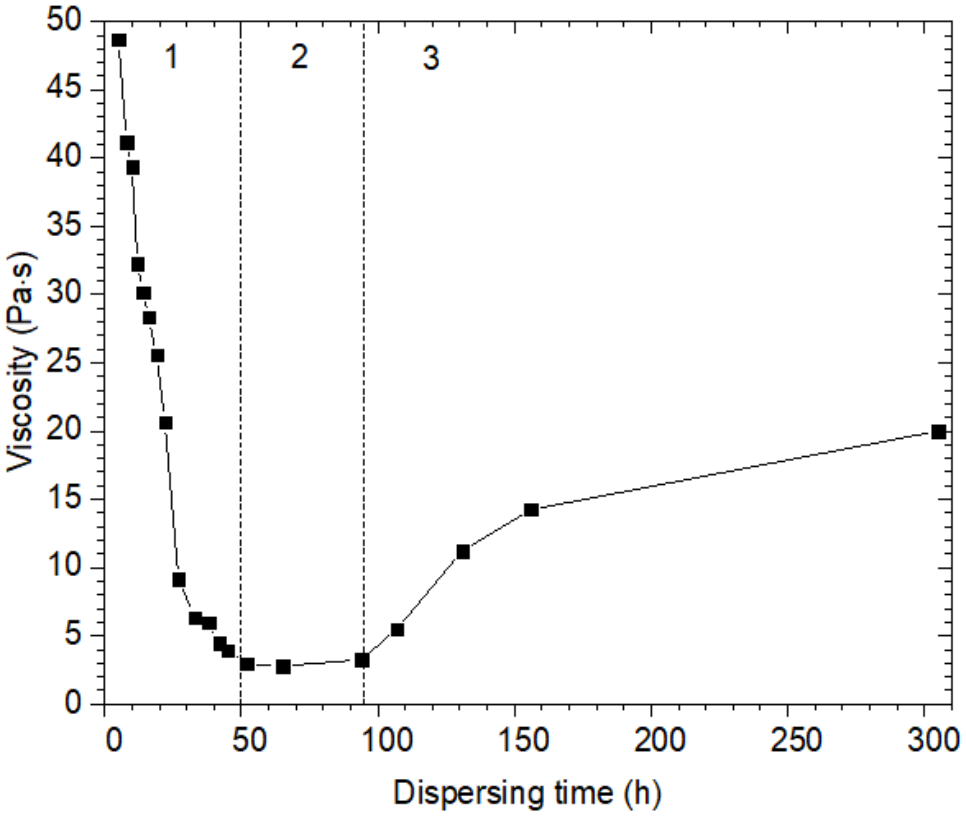

Figure 3.16 – Viscosity at 2 s^{-1} vs. dispersing time.

Three main zones can be clearly distinguished in this curve, regarding the viscosity tendency. Dotted lines were represented in Figure 3.16 to emphasize these three zones with their corresponding numbers 1, 2, and 3. These zones are related to the dispersing time, with the following criteria:

(1) Zone 1 – Dispersing time between 5 and 50 hours, where the viscosity decreases.

(2) Zone 2 – Dispersing time between 50 and 95 hours, where the viscosity remains constant;

(3) Zone 3 – Dispersing time between 95 and 305 hours, where the viscosity increases.

A decrease of the viscosity is observed in zone 1, which is more pronounced at the first 27 hours. Approaching zone 2, the decrease of the viscosity becomes more gradual. The preparations of the suspension were performed by adding all the components in a certain order: balls, dispersant, resin and LTCC powder. In this sense there is no previous step of mixing all the components. This means that the wetting of the powder occurs at the beginning of the dispersion process.

For short times, fewer than 5 hours, the balls could not move properly because the powder was not totally wetted by the liquid. Once the powder is wetted, and with the aid of the dispersant, the balls start moving in the jar following the milling system movement and the dispersion process takes place. Thus, the initial 5 hours is for the initial stage for the wetting of the powder.

After these 5 hours, the effect of the movement of the balls is more effective increasing the adsorption of the dispersant onto the particles surface and the particles de-agglomeration, resulting in a reduction of attractive interactions between particles. Once the attractive forces between particles are reduced, the viscosity of the system drastically decreases, as observed in the first stage of zone 1. The other evidence is that the most abrupt variation of the study takes place between 5 and 27 hours, starting with a viscosity of 48.67 Pa·s and decreasing until 9.15 Pa·s, representing a variation of 39.52 Pa·s. During this period, the viscosity of the system decreases 81.2 % with respect to the initial stage (5 hours), with a rate of 1.8 Pa·s/h. Another important factor that contributes to the drastic viscosity variation is that the balls' mobility increases by decreasing the viscosity, meaning more energy is added to the system and, therefore, the homogenization of the suspension is accelerated.

At the end of zone 1, between 27 and 52 hours, the viscosity continues decreasing but at a lower rate than the first stage, 0.25 Pa·s/h, reaching a minimum with an apparent viscosity

of 2.94 Pa·s. During these 25 hours the viscosity decreases 12.8 % more with respect to the first stage of zone 1, meaning a viscosity reduction of 94 in all of zone 1.

Zone 2 is defined as a constant zone, where the viscosity remains almost the same for a period of 40 hours approximately. In this zone the minimum viscosity is achieved with a value of 2.8 Pa·s. This means that in this zone the maximum dispersion of this system is achieved, i.e., the de-agglomeration of the particles is already accomplished and the dispersant absorption onto the particle surface reaches its maximum. In this regard, zone 2 is the period with the highest interest in terms of homogeneity and stability of the LTCC suspension, with a reduced amount of agglomerates and with the maximum absorption of the dispersant.

Zone 3 is defined between 95 and 305 hours of dispersing time, where the viscosity continuously increases with the dispersing time. The increase of the viscosity could be explained with the reduction of the particle size due to the effective milling of the particles, which is not the aim of this process. Thus, if the milling process is in fact milling the ceramic particles, more particle surface area is being created. However, the amount of dispersant remains the same during the whole experiment which leads to a reduction of the ratio between the dispersant and particle surface area.

The particle size measurements were performed at each dispersing time for its correlation with the viscosity measurements and cure depth. Figure 3.17 shows the particle size distribution in volume. These results show the particle size distribution of the initial powder and for the suspension with 8, 65, and 305 hours of dispersing time, associated to zone 1, zone 2, and zone 3, respectively.

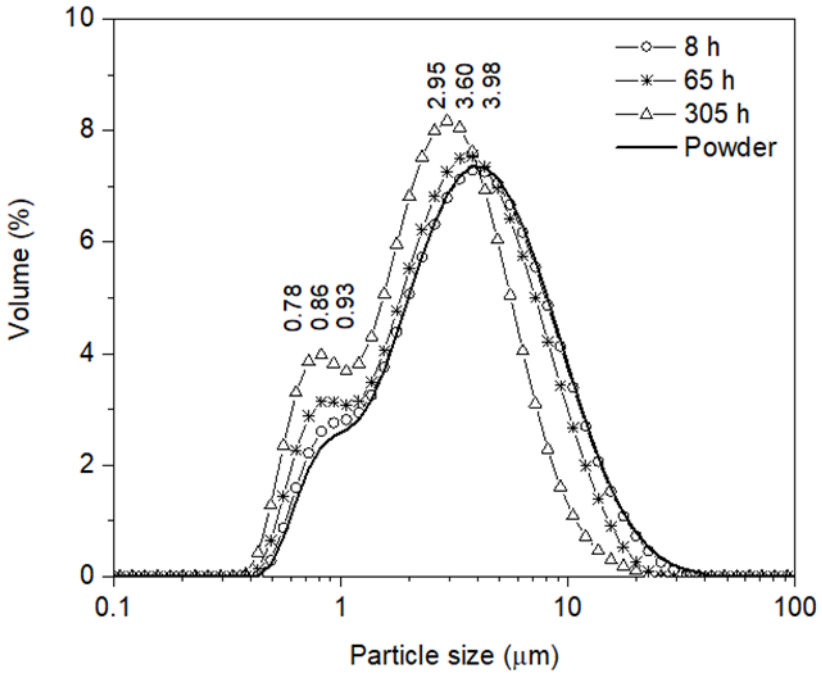

Figure 3.17 – Particle size distribution of the LTCC powder and of 8, 65, and 305 hours of dispersing time of the LTCC suspension.

A bimodal distribution of all particle size distributions is observed. From now on, the fraction with smaller values of particle size will be called fine fraction, and the population with larger particle size will be denominated as coarse fraction. Fine and coarse populations will be used to simplify the analyzing, However it does not refer exclusively to the primary particles, but also to the agglomerate/aggregate/particle with this size distribution. As the particle size distribution has a bimodal distribution, the analysis will be presented in terms of both fractions. The values presented in Figure 3.17 are the d_{50} of both particle size populations for the three different dispersing times.

The maximum value of particle size decreases with the dispersing time, from 30 µm (powder) to 20 µm for the samples with 65 and 305 hours of dispersing time. This means that the larger agglomerates/particles are being de-agglomerated/milled during this process. As a result, the particle size distribution is shifted to smaller values of particle size and becomes narrower as the dispersing time increases. Note that the minimum particle size remains almost the same and the volume percentage at d_{50} of both fractions increases with the dispersing time. Thus, two factors are being involved during the dispersing process: on one hand, the d_{50} of both fractions decreases due to the de-agglomeration and/or milling

of the agglomerates/particles and, on the other hand, the volume percentage at d_{50} increases once more superficial area is being formed with this de-agglomeration and/or milling.

The particle size was measured at different dispersing times during the 305 hours of the whole experiment. Figure 3.18 shows the viscosity curve in function of the dispersing time, the same explained previously, with the addition of the particle size of both fractions.

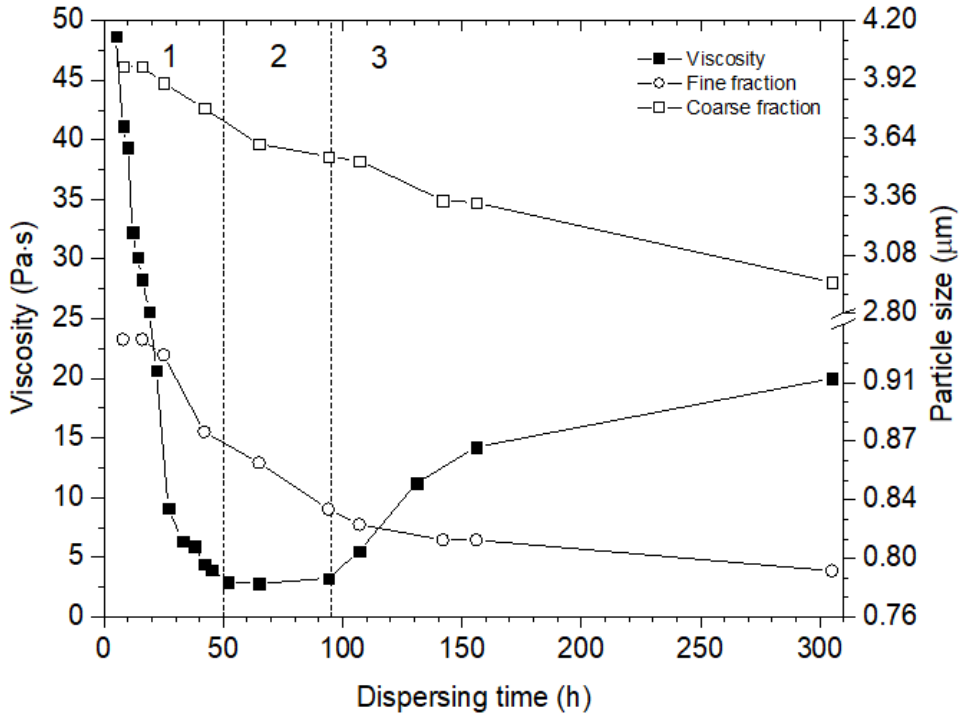

Figure 3.18 – Viscosity and particle size vs dispersing time.

It is observed that during the first 20 hours of zone 1 the particle size remains almost constant. Thus, the viscosity reduction is mostly associated with adsorption of the dispersant onto the particle surface. Nevertheless, between 20 and 60 hours, both particle fractions have a particle size reduction, increasing the specific surface area of the whole system. At the beginning of the dispersing process there is plenty of dispersant available in the system, thus the adsorption process onto the particles is faster when compared with the final stage of zone 1 (30-50 hours). In this sense, the abrupt decrease of the viscosity between 5 and 30 hours of dispersing time is related with the availability of the dispersant. In the final state

of zone 1, the amount of free dispersant is not as much as at the beginning of the dispersing process, resulting in a slower absorption rate of the dispersant. At the same time, more specific surface area is being generated by the de-agglomeration, decreasing the relative proportion of dispersant amount to superficial area.

In zone 2 the viscosity remains almost constant. However, in this zone the particle size of both fractions decreases 5.5 %, and as a result, more specific surface area is formed. Nonetheless, in this zone the viscosity value is the lowest of the whole study, which means that the mobility of the balls reaches its maximum, aiding the adsorption of the dispersant. In this regard, the viscosity remains constant during 40 hours due to the balance between the generation of new specific surface area and absorption rate of the dispersant onto the particle surface, which increases by the higher mobility of the balls in this zone.

In zone 3 the viscosity increases, explained by the lack of dispersant available for the new surface formed by the de-agglomeration and/or milling of the particles. Note that the particle size reduction of the fine fraction is more evident in zones 1 and 2 when compared with zone 3, which tend to a constant value of particle size. The total reduction of the fine fraction is around 16 %, from an initial d_{50} of 940 to 790 nm. However, the coarse fraction has a reduction of 15 % during zone 3, for a total particle size reduction of 26 %. This corresponds to a decrease in the median particle size from 3.98 to 2.95 μm, as a result of the de-agglomeration of the large agglomerates and/or milling of the large particles. Thus, the increase of the superficial area and the lack of dispersant leads to an increase in the viscosity value.

Figure 3.19 shows the volume percentage at d_{50} for both fractions and the curve of viscosity during the dispersing process.

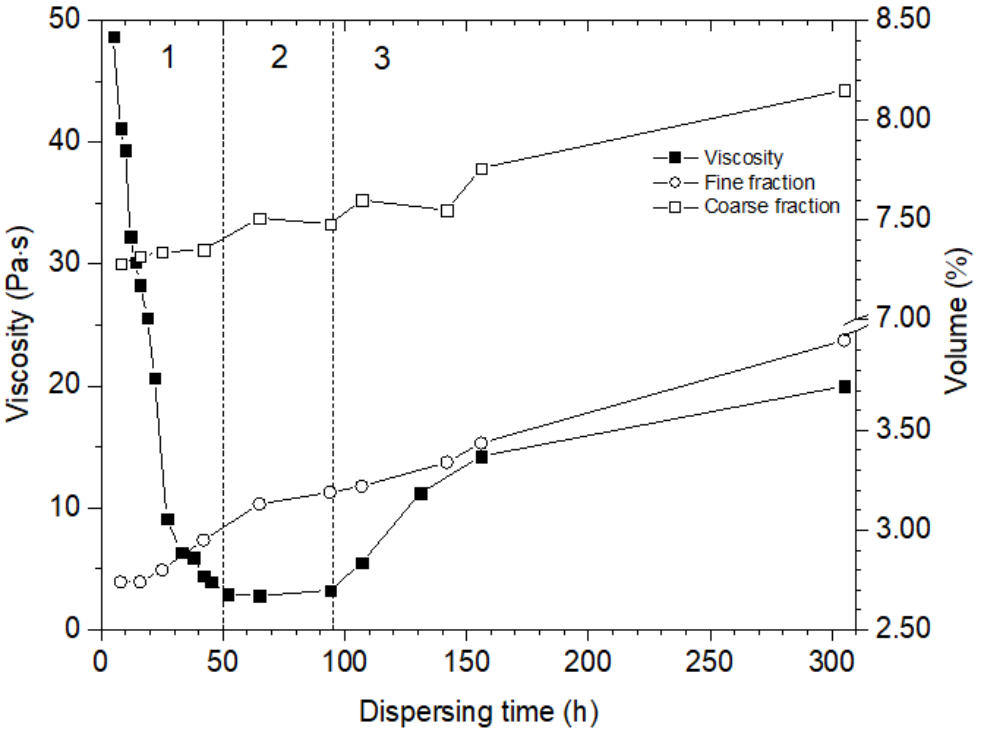

Figure 3.19 - Viscosity and volume percentage at d_{50} vs dispersing time

It is observed that in zone 1 the volume percentage of the fine fraction presents greater growth when compared with the coarse fraction which does not have a significant variation. This can be explained by the de-agglomeration of the coarse fraction which generates fine particles, representing an increase of 0.30 % of volume percentage of the fine fraction in this zone. Note that the volume percentage of the coarse fraction presents a gradual increase during the whole experiment, with a total increase of 0.90 %. In zone 2, the volume percentage of the fine fraction increases 0.20 % more, tending to a constant value. However, in zone 3 the volume percentage of the fine fraction increases again, reaching its maximum at 305 hours of dispersing time with a total of 1.20 % growth with respect to the initial volume percentage value. Accordingly, the volume of the fine fraction increases more than the coarse fraction which are related with the de-agglomeration and/or milling of the large particles and, consequently, the formation of more surface area.

3.5.2. Influence of particle size on photocuring behavior

The photocuring behavior was also studied during the dispersing process, analyzing the cure depth for the 305 hours. Figure 3.20 shows the cure depth measured at an energy dose of 140 mJ·cm^{-2}, which corresponds to 5 seconds of exposure time for the test setup configuration. The particle size for each dispersing time is also presented in this graphic to compare the effect of the particle size on the cure depth.

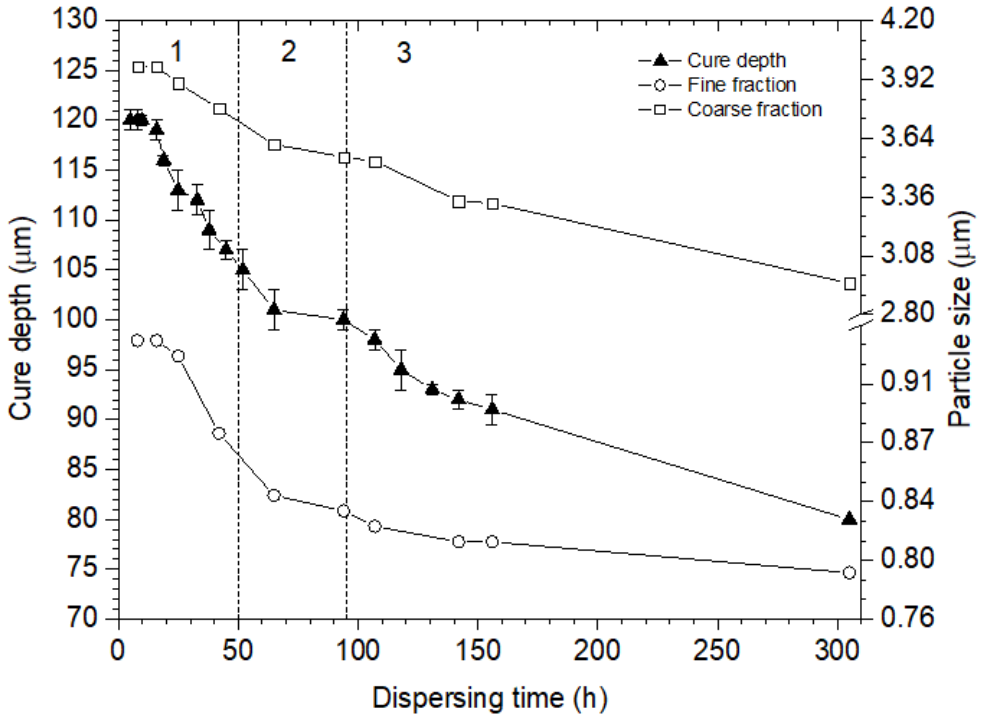

Figure 3.20 – Cure depth and particle size reduction vs dispersing time.

For the first 20 hours of zone 1, the cure depth is almost constant which agrees with the particle size result, i.e., no changes of particle size results in a constant cure depth with an average value of 120 µm. After the first 20 hours of the dispersing process, the cure depth decreases around 12.5 % following the particle size reduction.

In zone 2 the variation of the cured depth becomes more gradual than in zone 1. In this zone the cure depth still decreases in value following the particle size reduction with the dispersing time, representing a 4.2 % reduction in this zone. However, between 65 and 95

hours, the cure depth is almost constant, around 100 µm, supported by the particle size values, which does not present a significant change.

In zone 3 the cure depth gradually decreases until 80 µm at 305 hours. As the particle size decreases, the scattering of the light increases, which leads to the reduction of the cure depth.

Figure 3.21 shows the cure depth and the volume percentage at d_{50}, where the increase of the percentage of both fractions are correlated also with the decrease of the cure depth.

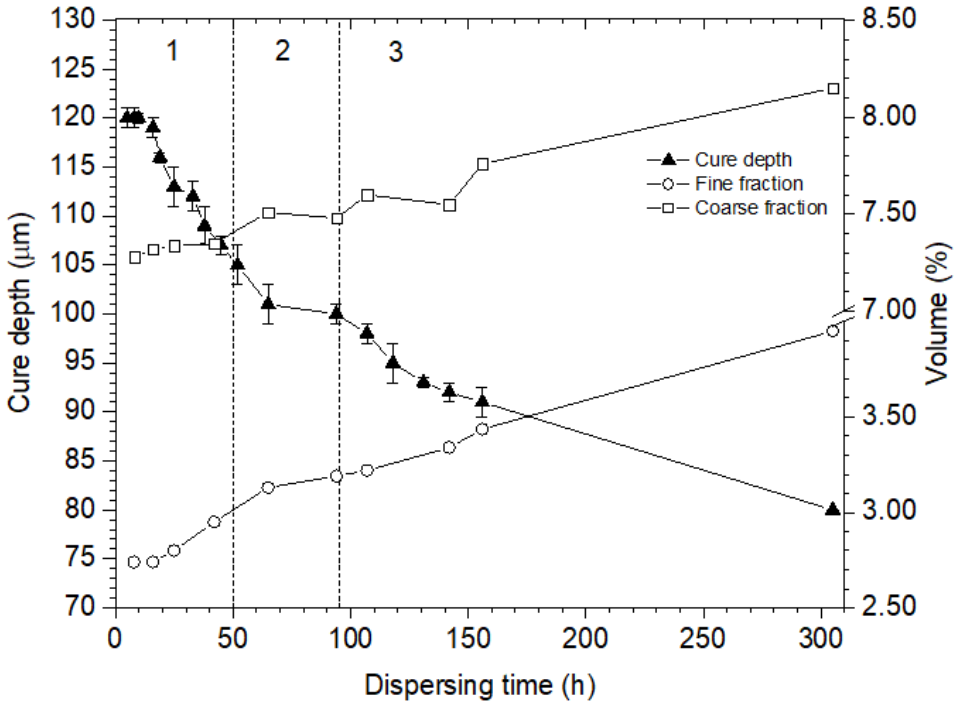

Figure 3.21 - Cure depth and volume percentage at d_{50} vs dispersing time.

The particle size reduction and the increase of the volume percentage at d_{50}, are related, i.e., the de-agglomeration and/or milling results in an increase in the amount of particle with smaller size. Thus, as the solid load is constant in this experiment, the particle size reduction means an increase in the number of particles with a higher specific surface area. From a perspective of light scattering, more scattering points are being generated during the dispersion process, resulting in lower cure depth values. In other words, the increasing of the light scattering is an impediment for the light to penetrate through the ceramic

suspension, limiting the polymerization of the resin. Therefore, the cure depth value decreases 33.3 % at 305 hours of dispersing time, with respect to the initial value of 120 µm.

To exemplify the difference in terms of E_c and the D_p at different dispersing times, one dispersing time was selected from the three different zones; 10 hours for zone 1, 65 hours for zone 2 and 305 hours for zone 3. To calculate these values, the cure depth was measured at different energy doses to graph the working curve of each sample, represented in Figure 3.22.

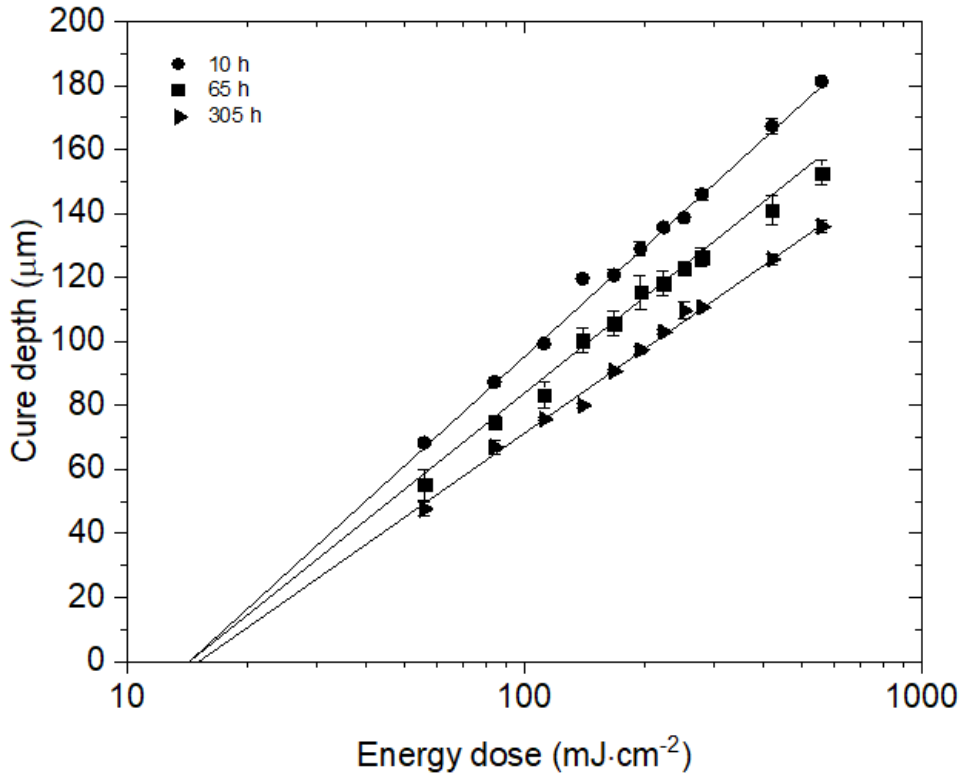

Figure 3.22 – Working curves for different dispersing time: 10, 65, and 305 hours.

E_c is almost the same for all curves: close to 15 mJ·cm^{-2}. However, D_p have different values: 49, 41, and 37 µm, respectively for 10, 65, and 305 hours of dispersing time. It is expected that the critical energy dose does not change, because this value is mainly affected by volume fraction of ceramic powder. However, a significant change of the slope is observed which results in a considerable variation of the sensitivity of the ceramic suspension. Applying the same energy dose to the suspension, a lower cure depth is achieved for the

samples with higher dispersion time. For example, to cure 150 µm, 10.5, 17, and 28.5 seconds of exposure time is needed to cure the same thickness, for 10, 65, and 305 hours of dispersing time, respectively. In this regard, the build velocity is also affected by the ceramic suspension characteristics. Nevertheless, the printing velocity will be not considered for the selection of the ceramic suspension procedure as the dispersing level and viscosity are not the same in all cases. However, depending on the final application, a smaller particle size distribution is required and in these cases the printing velocity decreases comparing to the same ceramic load. Moreover, as the particle size decreases, more scattering of the light occurs, and the resolution of the fine details also becomes a factor which should be considered.

Regarding both viscosity and photocuring behavior, the range of dispersing time selected for the large-scale production of the LTCC suspension was between 65 and 95 hours, within zone 2. At this range, the viscosity of the suspension reaches its minimum (2.8 Pa·s.at 2 s^{-1}) and, at the same time, the cure depth variation is almost constant (100 µm), representing the range where both factors remain almost constant. Once the LTCC suspension has almost the same characteristics in this dispersing time range, the dispersing time was selected at 65 hours, which represents less time consumption.

3.5.3. Stabilization of the LTCC suspension

In this section a final study of homogenization and stabilization of the final LTCC suspension is presented. Moreover, a comparison of the resin and the LTCC suspension is presented regarding both photocurable and rheological behavior.

During the preparation of the LTCC suspension, the formation of air bubbles is unavoidable, which may create defects during the printing process. Thus, the degassing of the suspensions is a crucial step of the process to avoid defect formation. This process was performed with a mixer system (Thinky – Planetary vacuum mixer) with a centrifuge system which reaches 2000 rpm and vacuum system. Thus, the air bubbles generated during the preparation of the LTCC suspension could be eliminated. Nevertheless, during the printing process the movement of the building platform can also introduce air into the suspensions. In this regard, an antifoam was used to aid the elimination of these air bubbles during the printing process.

After the 65 hours of dispersing time, the balls are separated from the ceramic suspension, as shown in Figure 3.23, and 0.4 wt.% with respect to the total weight of an antifoam (BYK 1794) is added to the suspensions. The addition of the antifoam is performed using the planetary vacuum mixer, over the course of 2 minutes, which promotes the homogenization of the antifoam and aids the degassing of the suspension. Figure 3.23 shows the final LTCC suspension on vat of the MIP-SLA machine, which will be further explained in chapter IV.

Figure 3.23 – image of a) removal method of the balls out of the LTCC suspension and b) LTCC suspension on the MIP-SLA machine.

The final LTCC suspension was studied in terms of its sedimentation for 5 months. The following results are related to the sedimentation test, which is performed to evaluate the stability of LTCC photocurable suspensions. Figure 3.24 shows a scheme used for the sedimentation evaluation. The LTCC suspension was dispensed into the measuring glass vials with a maximum height value of 3.5 cm and stored to rest in the dark. The sedimentation results are presented in term of resin percentage, i.e., resin height (h) with respect to the total height (H).

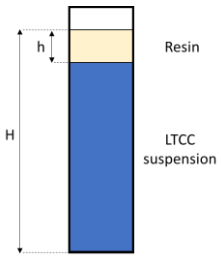

Figure 3.24 – Schematic diagram for the sedimentation test.

Figure 3.25 shows the results of the sedimentation test. It was observed that for times shorter than 30 days, the separation of both phases, resin and LTCC suspension, are not sufficiently clear to be measured. Thus, the measurements are presented for times longer than 30 days. However, some initial phase separation evidence was visually detected after 10 days.

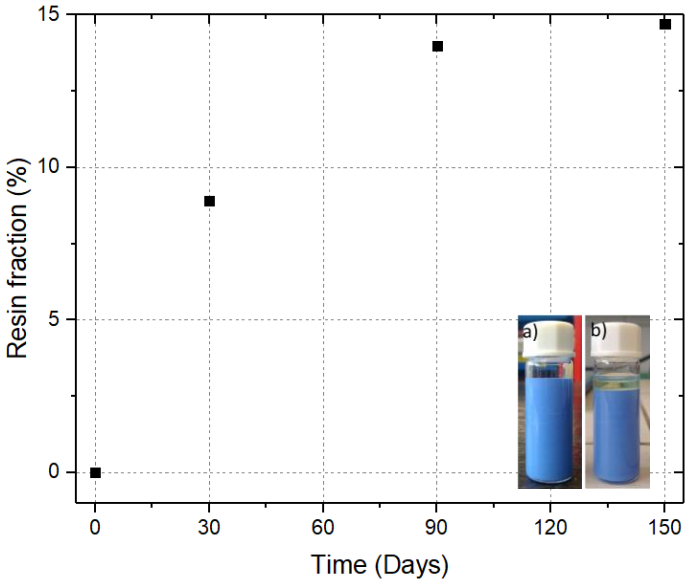

Figure 3.25 – Percentage of resin fraction vs time. Image a) and b) are related to the 0- and 150-day results, respectively.

Images a and b presented in Figure 3.25 correspond to the 0- and 150-day samples, respectively. It is observed that the percentage of the resin fraction increases as the time increases, as a result of the sedimentation of the LTCC particles. Moreover, the maximum of the resin fraction tends to be 15 %. The stability of the LTCC suspension is suitable for the printing process, once a phase separation is not detected during the first days. This means that the LTCC suspension could be used without sedimentation of the particles during the printing process.

The rheological properties and the procurable behavior were evaluated after the addition of the antifoam. Regarding the viscosity, the addition of the antifoam leads to an increase of the viscosity to values of 3.6 Pa·s at 2 s^{-1}, however it is still lower than the maximum value. Regarding the photocuring behavior, no significant changes were observed by adding the antifoam. Figure 3.26 shows the flow curves of the SPOT LV and the final suspension formulation with 67 wt.% of LTCC powder. An increase of two orders of magnitude of the viscosity is observed by adding the LTCC powder and, apart from that, the rheological behavior changes from Newtonian to pseudoplastic behavior.

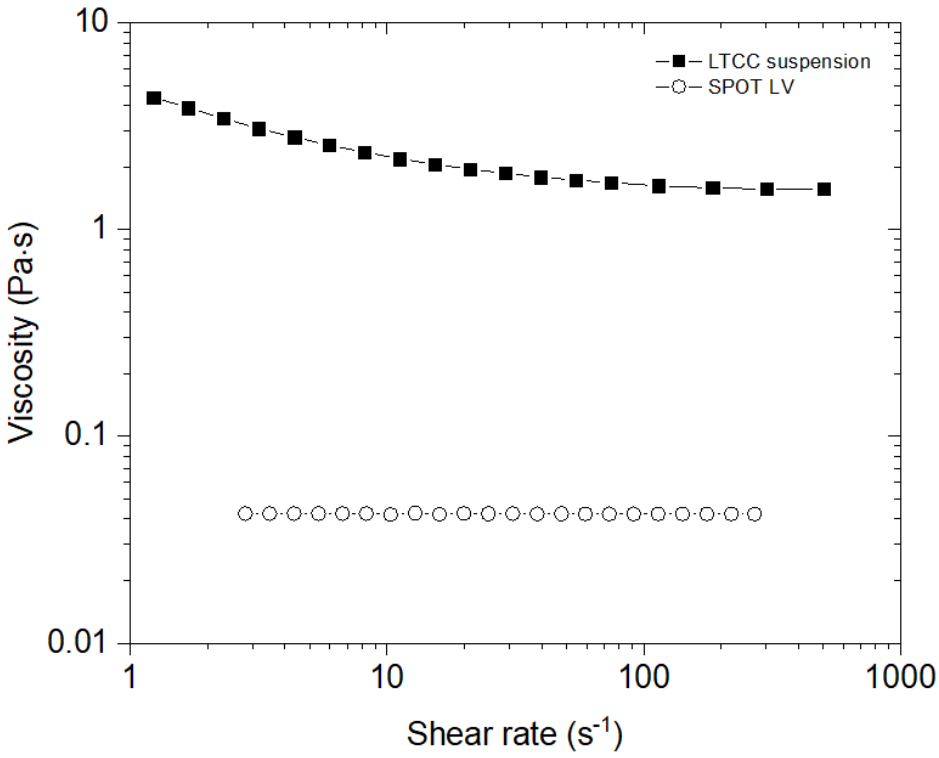

Figure 3.26 – Flow curves for the SPOT LV resin and for the optimized LTCC suspension.

Table 3.10 shows the results of the Herschel-Bulkley fitting for the SPOT LV resin and for the final suspension formulation with 67 wt.%. The SPOT LV has index flow and yield stress values close to zero, demonstrating Newtonian behavior. On the other hand, the final suspension has pseudoplastic behavior, favorable to prevent/delay the sedimentation process, with a yield stress of 3.3 ± 0.1.Pa. Regarding the reported values, 185 mPa[26] , this value is relatively high, nevertheless it is suitable for the developed MIP-SLA machine.

Table 3.10 – Herschel-Bulkley fitting results for SPOT LV and for the optimized LTCC suspension.

Viscosity parameters	SPOT LV	LTCC suspension
τ_0 (Pa)	0.07 ± 0.03	3.3 ± 0.1
K (Pa·s^n)	0.0394 ± 0.0023	2.2 ± 0.1
n	1.0385 ± 0.0116	0.929 ± 0.002
Adj. R-Square	0.99928	0.99984

Figure 3.27 shows the comparison of the working curve of the SPOT LV resin and the final LTCC ceramic suspension. There is a clear change of the photocuring behavior by adding the 67 wt.% of ceramic powder.

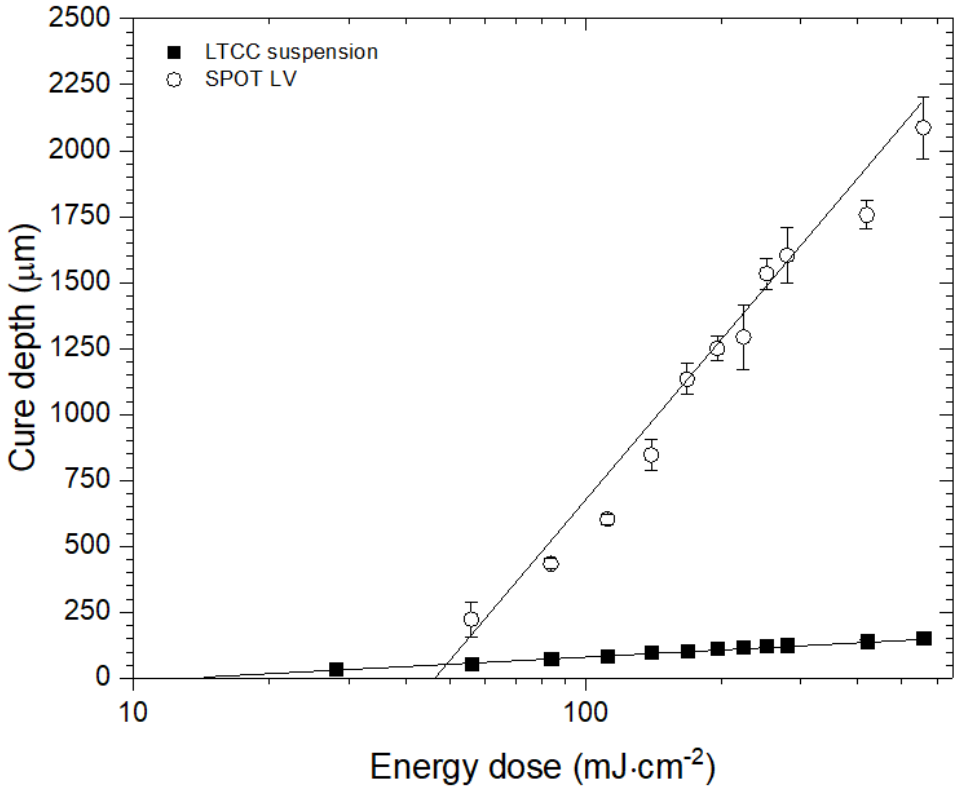

Figure 3.27 – Working curves of the SPOT LV resin and for the optimized LTCC suspension.

Table 3.11 shows the critical energy dose and the sensitivity for both samples. By adding the ceramic powder, the sensitivity and the critical energy dose decreases for the reasons mentioned above.

Table 3.11 - Critical energy dose and sensitivity for the SPOT LV resin and for the optimized LTCC suspension.

Photocurable parameters	SPOT LV	LTCC suspension
D_p (µm)	850	41
E_c (mJ·cm^{-2})	48	15

In order to evaluate the reuse of the LTCC suspensions after 5 months, a mechanical stirring of the suspension was performed and evaluated. The results show that the re-dispersing of the LTCC suspension is feasible ensuring the same results in terms of rheology and particle size distribution, and photocuring behavior could be obtained.

Conclusions

The development and optimization of a LTCC suspension has been discussed in this chapter, based on the inherent requirements of the selected AM technology, i.e., viscosity lower than 5 Pa·s (at 2 s^{-1}) and high sensitivity to visible light, maximizing the solid load for further thermal treatment.

To accomplish these aims, an initial study of the dispersing medium based on photocurable resins was shown. Is was concluded that the spot-lv resin is the resin with the optimal balance between photocuring and rheological behavior.

The influence of the solid load was analyzed in terms of both photocuring and rheological behavior. The energy dose necessary to initiate the photopolymerization process (the critical energy dose) decreases for larger concentrations of ceramic powder. On the other hand, the sensitivity parameter decreases as a result of the addition of ceramic particles. Thus, the higher the solid load the lowest the sensitivity of the LTCC suspension.

Regarding the rheological behavior, it was demonstrated that the addition of ceramic powder drastically increases the viscosity, with it being more evident for volume fractions larger than 72 wt.%. the ceramic suspensions present a proper photocuring behavior for the MIP-SLA machine. However, the maximum viscosity for the MIP-SLA technology is 5 Pa·s (At 2 s^{-1}), therefore, although the photocuring behavior is appropriate for all studied suspensions, the viscosity must also be suitable for the printing process.

In this regard, after the dispersant concentration and dispersing time optimization, the maximum solid load was established at 67 wt.% LTCC with a 1.5 wt.% of dispersant, with respect to the solid load, with a viscosity of 4.5 Pa·s at 2 s^{-1}.

Furthermore, based on the previous results, the dispersing time was optimized for large-scale production in a horizontal ball mill. It was demonstrated that the viscosity of the suspension decreases during the dispersing process. The optimal dispersing time, which corresponds to the minimum viscosity, was achieved in a range of 50 to 95 hours, with a viscosity of 2.8 Pa·s at 2 s^{-1}. For higher dispersing time, the viscosity increases due to the

particle size reduction and lack of dispersant for the new particle surface area. Moreover, the particle size reduction leads to an increase in light scattering, which attenuates the penetration of the light through the ceramic suspension, limiting the polymerization of the resin. In this regard, a decrease of the sensitivity of the suspensions was observed as the particle size decreases. However, as the volume of LTCC particles is constant along the experiment, the critical energy dose remains constant.

It was demonstrated that the addition of an antifoam into the formulation improves air bubble elimination, slightly increasing the viscosity and maintaining photocuring behavior of the LTCC suspension. The stability of the suspensions was analyzed for five months and, although the suspensions presented an evident sedimentation, it was demonstrated that the optimized LTCC suspension could be reused after the five months. The recuperation of the optimized LTCC suspension was achieved applying a mechanical stirring, ensuring the same results in terms of rheology, particle size distribution, and photocuring behavior.

The optimized LTCC suspension has a viscosity of 3.6 Pa Pa·s at 2 s^{-1}, meaning a viscosity 90 times higher than the spot-lv resin without ceramic particles. On the other hand, the sensitivity decreases 95 % with the addition of the ceramic particles: the sensitivity is 850 µm for the resin and 41 µm for the optimized LTCC suspension. Concerning the critical energy dose, the values obtained were 48 $mJ \cdot cm^{-2}$ for the resin and 15 $mJ \cdot cm^{-2}$ for the LTCC suspension, meaning a reduction of 69 % of the energy needed to initiate the polymerization process when the ceramic particles are added.

.

References

[1] K. Holmberg, *Handbook of applied surface and colloid chemistry*, 2nd ed., vol. 1. JOHN WILEY & SONS, LTD, 2002.

[2] P. Boch and J.-C. Niepce, *Ceramic Materials: Processes, Properties and Applications*, 1st ed. ISTE, 2001.

[3] K. Ohenoja, "PhD Dissertation: Particle size distribuition and suspension stability in aqueous submicron grinding of $CaCO_3$ and TiO_2," University of Oulu, 2014.

[4] H. Liao, "PhD Dissertation: Stereolithography Using Compositions Containing Ceramic Powders," University of Toronto, 1997.

[5] R. M. Botella, *Reología de suspensiones cerámicas*. Madrid: Consejo superior de investigaciones científicas, 2015.

[6] U. Paik, V. A. Hackley, S.-C. Choi, and Y.-G. Jung, "The effect of electrostatic repulsive forces on the stability of BaTiO3 particles suspended in non-aqueous media," *Colloids Surf.*, vol. 135, pp. 77–88, 1998.

[7] C. Eisermann, M. R. Mallembakam, C. Damm, W. Peukert, S. Breitung-Faes, and A. Kwade, "Polymeric stabilization of fused corundum during nanogrinding in stirred media mills," *Powder Technol.*, vol. 217, pp. 315–324, 2012.

[8] T. Ring, "Colloid Stability of Ceramic Suspensions," in *Fundamentals of Ceramic Powder Processing and Synthesis*, Fundamenta., 1996, pp. 421–489.

[9] J. N. Israelachvili, *Intermolecular and Surface Forces*, Third edit. 2011.

[10] P. Somasundaran, S. C. Mehta, X. Yu, and S. Krishnakumar, "Colloid Systems and Interfaces Stability and Surfactant Adsorption," in *Handbook of Surface and Colloid Chemistry*, 2009, pp. 155–194.

[11] A. Badev *et al.*, "Photopolymerization kinetics of a polyether acrylate in the presence of ceramic fillers used in stereolithography," *J. Photochem. Photobiol. A Chem.*, vol. 222, pp. 117–122, 2011.

[12] T. Chartier, A. Badev, Y. Abouliatim, P. Lebaudy, and L. Lecamp, "Stereolithography process : Influence of the rheology of silica suspensions and of the medium on polymerization kinetics – Cured depth and width," *J. Eur. Ceram. Soc.*, vol. 32, pp. 1625–1634, 2012.

[13] S. Zürcher and T. Graule, "Influence of dispersant structure on the rheological properties of highly-concentrated zirconia dispersions," *J. Eur. Ceram. Soc.*, vol. 25, pp. 863–873, 2005.

[14] F. Ramos, "PhD Dissertation: Integración de la tecnología cerámica multicapa," University of Barcelona, 2014.

[15] P. Baláž, "High-Energy Milling," in *Mechanochemistry in Nanoscience and Minerals Engineering*, Springer, 2008, pp. 103–129.

[16] A. Licciulli, C. E. Corcione, A. Greco, V. Amicarelli, and A. Maffezzoli, "Laser stereolithography of ZrO_2 toughened Al_2O_3," *J. Eur. Ceram. Soc.*, vol. 24, pp. 3769–3777, 2004.

[17] C. Hinczewski, S. Corbel, and T. Chartie, "Ceramic Suspensions Suitable for Stereolithogiaphy," *J. Eur. Ceram. Soc.*, vol. 18, pp. 583–590, 1998.

[18] T. Hafkamp, G. Van Baars, B. de Jager, and P. Etman, "A trade-off analysis of recoating methods for vat-photopolymerization of ceramics," in *Proceedings of the 28th Annual International Solid Freeform Fabrication Symposium*, 2017, pp. 687–711.

[19] H. Liao, "PhD Dissertation: Stereolithography using compositions containing ceramic powders," University of Toronto, 1997.

[20] A. Goswami, K. Ankit, N. Balashanmugam, A. M. Umarji, and G. Madras, "Optimization of rheological properties of photopolymerizable alumina suspensions for ceramic microstereolithography," *Ceram. Int.*, vol. 40, pp. 3655–3665, 2014.

[21] P. J. Bártolo, *Stereolithography:Materials, Processes and Applications*. Springer, 2011.

[22] K. Taki, Y. Watanabe, T. Tanabe, H. Ito, and M. Ohshima, "Oxygen concentration and conversion distributions in a layer-by-layer UV- cured film used as a simplified model of a 3D UV inkjet printing system," *Chem. Eng. Sci.*, vol. 158, pp. 569–579, 2017.

[23] Q. Lian, F. Yang, H. Xin, and D. Li, "Oxygen-controlled bottom-up mask-projection stereolithography for ceramic 3D printing," *Ceram. Int. J.*, vol. 43, pp. 14956–14961, 2017.

[24] J. W. Halloran, “Ceramic Stereolithography: Additive Manufacturing for Ceramics by Photopolymerization,” *Annu. Rev. Mater. Res.*, vol. 46, pp. 19–40, 2016.

[25] P. F. Jacobs, “Fundamentals of stereolithography,” *3D Syst.*, pp. 196–210, 1992.

[26] M. L. Griffith and J. W. Halloran, “Freeform Fabrication of Ceramics via Stereolithography,” *J. Am. Ceram. Soc.*, vol. 79, pp. 2601–2608, 1996.

[27] J. Deckers, J. Vleugels, J. Kruth, and I. Introduction, “Additive Manufacturing of Ceramics: A Review,” *J. Ceram. Sci. Technol.*, vol. 260, pp. 245–260, 2014.

[28] G. Mitteramskogler *et al.*, “Light curing strategies for lithography-based additive manufacturing of customized ceramics,” *Addit. Manuf.*, vol. 1–4, pp. 110–118, 2014.